附件 1　　浙江水利水电学院“南浔学者”申请表

<table>
<tr><td>姓　名</td><td>王立强</td><td>出生年月</td><td>1980 年 12 月</td><td>参加工作时间</td><td>2010 年 12 月</td></tr>
<tr><td>现所在单位(部门)</td><td>机械与汽车工程学院</td><td>最高学历/学位</td><td>研究生/博士</td><td>专业技术职务</td><td>讲师/工程师</td></tr>
<tr><td>拟申报类别</td><td colspan="5">三类学者</td></tr>
<tr><td>符合条款</td><td colspan="5">符合三类学者业绩成果（1）主持省部级教学科研纵向项目 2 项：VI 类项目 2 项，绩点 60；发表 5 类论文（SCI 期刊论文）3 篇，绩点 60。总绩点 120。</td></tr>
<tr><td rowspan="8">所涉业绩</td><td rowspan="2">教学类
绩点：_____</td><td colspan="4"></td></tr>
<tr><td colspan="4"></td></tr>
<tr><td rowspan="2">科研类
绩点：120</td><td colspan="4">符合 VI 类项目 2 项：2017C33160 / LGF20E070001</td></tr>
<tr><td colspan="4">5 类论文 3 篇: SCI 期刊论文 3 篇</td></tr>
<tr><td rowspan="2">人才称号类
绩点：_____</td><td colspan="4"></td></tr>
<tr><td colspan="4"></td></tr>
<tr><td rowspan="2">与上述水平相当的其他业绩</td><td colspan="4"></td></tr>
<tr><td colspan="4"></td></tr>
<tr><td>总绩点</td><td colspan="4">120</td></tr>
<tr><td colspan="5">备注：请严格按照《浙江水利水电学院“南浔学者”实施办法（试行）》（浙水院〔2022〕113 号）附件《业绩成果绩点赋值项目库》的类目、分类、等级（等次）、绩点填写。</td></tr>
<tr><td>个人承诺</td><td colspan="5">本人承诺上述所填内容真实、准确；如有不实，本人承担相应责任。
签名：王立强　时间：2022.11.22</td></tr>
<tr><td colspan="6">以上部分由申请人填写，所在单位审核。以下由单位（部门）和学校填写。</td></tr>
<tr><td>所在单位
（部门）意见</td><td colspan="5">1.经审核，申请人所填内容：□属实　□不属实；
2.是否符合所申请的类别：□符合　□不符合；
3.是否同意推荐：□同意　□不同意。
负责人签名：　（部门盖章）
____年____月____日</td></tr>
<tr><td>科技处审核
意见</td><td colspan="2">负责人签名：　（部门盖章）
年___月___日</td><td>教务处审核
意见</td><td colspan="2">负责人签名：　（部门盖章）
年___月___日</td></tr>
<tr><td>其他相关职能
部门审核意见</td><td colspan="5">负责人签名：　（部门盖章）
_____年____月____日</td></tr>
<tr><td>学校意见</td><td colspan="5">（学校盖章）
____年____月____日</td></tr>
</table>

备注：表格请用 A4 纸打印，有关佐证材料附后。

Original Research Article

Institution of MECHANICAL ENGINEERS
Journal of MECHANICAL ENGINEERING SCIENCE

Proc IMechE Part C:
J Mechanical Engineering Science
2022, Vol. 236(11) 5785–5795

DOI: 10.1177/09544062211063130
journals.sagepub.com/home/pic
SAGE

Feedforward-control-based nonlinear control for overhead cranes with matched and unmatched disturbances

Liqiang Wang[1], Xianqing Wu[2] and Meizhen Lei[2,3]

Abstract

In this paper, a composite control method consisting of a feedforward control method and a sliding mode control method is proposed for control of the overhead crane. For existing methods, only matched disturbances are taken into consideration, unmatched disturbances are usually neglected. To address this drawback, a disturbance compensation method is constructed to attenuate the effects of disturbances and a continuous global sliding mode control method is devised to guarantee the stability. More precisely, we first make some transformations on the original model. Then, a disturbance compensation method is proposed and a continuous global sliding mode control scheme is introduced straightforwardly. The stability of the closed-loop system and the convergence of the states are proven through complete theoretical analysis. Finally, simulation and experimental tests are carried out to illustrate the regulation control property of the designed approach as well as its excellent disturbance rejection characteristic.

Keywords

underactuated system, overhead crane, unmatched disturbance, disturbance compensation, sliding mode control

Introduction

Underactuated mechanical systems are widely utilized in many industrial sites, the control of which has received a lot of attention over the past several decades.[1–13] As a commonly found underactuated system, overhead cranes are also widely used for their merits such as high efficiency, great load capacity, and less energy consumption. For crane systems, the major task is to move cargos from one position to another position. One inherent problem limiting their efficiency is that the cargo cannot be controlled directly by the control input. Therefore, the underactuated characteristic that fewer control inputs than variables to be controlled makes the automation control of the overhead crane much more challenging.

Literature review

During the past few decades, abundant efforts have been made to solve the control issues of the overhead cranes. Many results have been reported on the regulation control of cranes. These results can be divided into open-loop and closed-loop categories. One representative open-loop method is input shaping theory, which has been proven to be valid on cranes for reducing the payload swing.[14–16] Some other open-loop approaches like trajectory planning methods also have been reported in the literature.[17,18] However, these methods are designed based on the exact knowledge of system parameters and the linearized system model. As a consequence, the control performance of these methods is easily affected by uncertain system parameters, different initial conditions, and external disturbances. For these reasons, owing to the robustness of feedback control against uncertainties, numerous works have been done. Specially, several control methods are proposed based on the Lyapunov theory.[19–22] Considering the system parameter variations, some adaptive control laws are designed, which could estimate system parameters based on some online update mechanism.[23–27] In addition, on the basis of the exact system information, some other interesting control methods are also developed for the crane control, which mainly include partial feedback linearization,[28–30] model predictive control,[31,32] and so on.[33–35]

All of the above mentioned works focus on the regulation control of the overhead crane system; uncertainties and external disturbances are ignored when making the control design. However, uncertainties and external disturbances are unavoidable in practical applications. For this case, considering the robustness of the sliding mode control technique with regard to uncertain disturbances, many sliding mode control approaches are developed for the disturbance rejection of the

[1]Faculty of Mechanical and Automotive Engineering, Zhejiang University of Water Resources and Electric Power, Hangzhou, China
[2]Faculty of Mechanical Engineering and Automation, Zhejiang Sci-Tech University, Hangzhou, China
[3]Suzhou Industrial Technology Research Institute of Zhejiang University, Suzhou, China

Corresponding author:
Xianqing Wu, Faculty of Mechanical Engineering and Automation, Zhejiang Sci-Tech University, NO. 928, Road Two, Xiasha District, Hangzhou 310018, China.
Email: wxq@zstu.edu.cn.

crane system. Specifically, Almutairi and Zribi investigate a sliding mode control law for the position regulation and anti-swing control of the crane system.[36] By combining partial feedback linearization and sliding mode control techniques, Tuan et al. proposed a nonlinear controller for the overhead crane system.[37] Sun et al. constructed a new sliding manifold and employed a sliding mode control scheme to guarantee the state convergence.[38] However, in order to eliminate the effects of uncertain disturbances, the switching gains of these sliding mode control methods should be chosen large enough. It is well known that there exists the chattering problem for these methods, which may lead to some undesired problems. Zhang et al. utilized the disturbance compensation technique to reduce the effects of the disturbances, and a finite-time control scheme is proposed. However, the swing elimination task is not taken into consideration when making control design.[39] In addition, from the theoretical viewpoint, for the existing robust control methods, only matched external disturbances that exist in the same channel as that of the control input are taken into account, and unmatched disturbances are neglected.[40–44]

Motivation and incitement

After carefully summarizing the existing approaches for the overhead crane, the following issues are still in existence and need to be solved or require further improvements.

- The reported sliding mode control approaches for the overhead crane system are discontinuous and have the chattering problem, which may lead to performance degradation or even system damage.
- Only matched disturbances are taken into consideration when making control design, that is, existing control methods are proposed on the basis of the assumption that the disturbances existing in the crane system satisfy the so-called matching condition.

In order to deal with these issues, inspired by the development of disturbance compensation control,[45–47] the disturbance compensation control technique is employed to attenuate the effects of uncertain disturbances in this paper.

Contribution and paper organization

This study seeks to design a nonlinear control scheme that guarantees the state convergence, maintains its control performance in the presence of matched and unmatched disturbances, and does not need to linearize the dynamic model near the equilibrium point. To achieve these objectives, a continuous global sliding mode control method, along with a disturbance estimator, is designed for the overhead crane. In particular, we first introduce the dynamic model of the crane system, make some model transformations, and describe the control objective. Then, a nonlinear disturbance estimator is proposed, a continuous global sliding mode control approach is devised, and detailed stability analysis is given. The availability and robustness of the devised control approach is verified via simulation and hardware experimental tests. Compared with existing methods for the crane control, the proposed control method here exhibits the following remarkable features:

1. Different from most existing disturbance rejection approaches, the proposed disturbance observer belongs to a feedforward control method, which is an effective solution and can attenuate the effects of disturbances from the system output.
2. The proposed sliding mode control method is continuous and global robustness against external disturbances, which is of significant importance in the engineering sense.
3. Both matched and unmatched disturbances are taken into consideration, which is more realistic for practical mechatronic systems.

The main work of this paper is outlined as follows. In the second section, the dynamic model is provided and some transformations are made. Then, in the third section, the main results are introduced, which include the disturbance observer design, continuous sliding mode control design, and stability analysis. Simulation and experimental results are provided in the fourth and fifth sections, respectively. Finally, some conclusions are made.

Dynamic Model

In this paper, the regulation and disturbance suppression control of the two-dimensional (2-D) underactuated overhead crane system is considered, and the dynamic equations of the overhead crane are[19,32,38]

$$(M+m)\ddot{x} + ml\ddot{\theta}\cos\theta - ml\dot{\theta}^2\sin\theta = F + d_1 \tag{1}$$

$$ml^2\ddot{\theta} + ml\ddot{x}\cos\theta + mgl\sin\theta = d_2 \tag{2}$$

where $x(t)$ is the cart displacement, $\theta(t)$ denotes the payload swing angle, M is the cart mass, m is the cargo mass, l is the rope length, g is the gravity acceleration, $F(t)$ is the control input, and $d_1(t)$ is the matched lumped disturbance term including frictions, unmodeled dynamics, uncertain disturbances, and so on, which exists in the same channel as that of the control input, $d_2(t)$[1] is the unmatched lumped disturbance term that acts on the different channel from the control input.

Before proceeding to the control development, some transformations are made with respect to the original dynamic equation (1) and equation (2). On the basis of equation (1) and equation (2), the following equations can be obtained

$$F = \mu_u u - ml\dot{\theta}^2\sin\theta - (M+m)g\tan\theta \tag{3}$$

$$\ddot{x} = -g\tan\theta - l\ddot{\theta}\sec\theta + d_2\sec\theta/ml \tag{4}$$

where the expressions of $u(t)$ and $\mu_u(t)$ are

$$u(t) = \ddot{\theta} + \mu_d \tag{5}$$

$$\mu_u(t) = -(M + m\sin^2\theta)l\sec\theta \tag{6}$$

$$\mu_d(t) = \frac{d_1\cos\theta}{(M+m\sin^2\theta)l} - \frac{d_2(M+m)}{(M+m\sin^2\theta)ml^2} \tag{7}$$

Then, the following auxiliary signals are introduced[48]

$$x_1 = x + l\ln(\sec\theta + \tan\theta),\ x_2 = \dot{x}_1 \tag{8}$$

$$x_3 = -g\tan\theta,\ x_4 = \dot{x}_3 \tag{9}$$

On this basis, one can rearrange equation (4) as

$$\begin{cases} \dot{x}_1 = x_2 \\ \dot{x}_2 = x_3 + \mu(x_3, x_4) \\ \dot{x}_3 = x_4 \\ \dot{x}_4 = -g\sec^2\theta\left(u - \mu_d + 2\dot{\theta}^2\tan\theta\right) \end{cases} \tag{10}$$

where $\mu(x_3, x_4)$ is an auxiliary function and the expression of which is

$$\mu(x_3, x_4) = -\frac{lx_3x_4^2}{(g^2 + x_3^2)^{3/2}} + \frac{d_2\sqrt{g^2 + x_3^2}}{mlg} \tag{11}$$

and $u(t)$ is considered as the control input of the new system model equation (10). For the practical overhead crane, the control objectives mainly include two tasks. One is that the cart needs to be driven from one position to another preset position quickly and safely. The other one is that the payload swing should be eliminated as the cart arrives at the target location. The control objectives can be formulated by

$$\lim_{t\to\infty} x(t) = p_d,\ \lim_{t\to\infty}\theta(t) = 0 \tag{12}$$

where p_d is the desired location of the trolley. From equation (8), equation (9), and equation (12), one can find that the control objectives in equation (12) are equivalent to

$$\lim_{t\to\infty} x_1(t) = p_d,\ \lim_{t\to\infty} x_3(t) = 0 \tag{13}$$

To achieve these control objectives, the following variables are constructed

$$e_1 = x_1 - p_d,\ e_2 = x_2,\ e_3 = x_3,\ e_4 = x_4 \tag{14}$$

Then, the system model equation (10) can be converted into the following form

$$\begin{cases} \dot{e}_1 = e_2 \\ \dot{e}_2 = e_3 + \mu(e_3, e_4) \\ \dot{e}_3 = e_4 \\ \dot{e}_4 = -g\sec^2\theta\left(u - \mu_d + 2\dot{\theta}^2\tan\theta\right) \end{cases} \tag{15}$$

where $\mu(e_3, e_4)$ denotes the following auxiliary function

$$\mu(e_3, e_4) = -\frac{le_3e_4^2}{(g^2 + e_3^2)^{3/2}} + \frac{d_2\sqrt{g^2 + e_3^2}}{mlg} \tag{16}$$

with the upper bound of $\varsigma \in \mathbb{R}^+$. The dynamic model equation (15) will be utilized in the following controller design and stability analysis.

Remark 1. At present, it is challenging for a disturbance-observer-based control method to deal with the control of the overhead crane system with nonvanishing unmatched disturbances. In the future, we will concentrate our attention on developing disturbance-observer-based control methods for the crane system in the presence of nonvanishing unmatched disturbances.

Main results

In this section, based on the obtained dynamic model equation (15), a nonlinear disturbance observer will be designed. Meanwhile, a continuous global sliding mode control scheme is introduced and the corresponding stability analysis is provided.

Disturbance observer design

In order to compensate uncertain disturbances through a feedforward control way, a nonlinear disturbance observer will be investigated. To begin with, the fourth equation of equation (15) is rewritten as the following form

$$\dot{e}_4 = f_u + f_d + f_f \tag{17}$$

where $f_u(t)$ is considered as the control input and $f_f(t)$ is an auxiliary function, whose expressions are

$$f_u = -gu\sec^2\theta,\ f_f = -2g\sec^2\theta\dot{\theta}^2\tan\theta \tag{18}$$

and $f_d(t)$ is considered as the uncertain disturbance with the bounds that $|f_d| \le v_p, |\dot{f}_d| \le v_d$ ($v_p, v_d \in \mathbb{R}^+$ denote prior known constants). We assume that $f_d(t)$ is unknown and needs to be estimated. To achieve the disturbance estimation objective, based on equation (17), a linear filter is introduced

$$\psi = e_4 + \alpha e_3 \tag{19}$$

where $\alpha \in \mathbb{R}^+$ is a control parameter. Then, based on equation (17) and the linear filter equation (19), and inspired by recently proposed disturbance-observer control methods,[45–47] the following disturbance observer is constructed

$$\hat{f}_d = \varepsilon_1 + \varepsilon_2 \tag{20}$$

$$\dot{\varepsilon}_1 = -\lambda\left(\varepsilon_1 + \varepsilon_2 + f_u + f_f + \alpha e_4\right) \tag{21}$$

$$\varepsilon_2 = \lambda\psi \tag{22}$$

wherein $\hat{f}_d(t)$ is the estimated disturbance, ε_1, ε_2 are auxiliary variables, and $\lambda \in \mathbb{R}^+$ is an observer gain.

Theorem 1. Under the designed disturbance observer equations (20)–(22), the time derivative of the observation error between the real disturbance and the estimated disturbance is always kept in a range in the sense that

$$\lim_{t\to\infty}\left|\dot{\tilde{f}}_d(t)\right| \le 2v_d \tag{23}$$

where $\tilde{f}_d(t) = f_d(t) - \hat{f}_d(t)$ is defined as the disturbance observation error.

Proof: First, taking the time derivative of $\tilde{f}_d(t)$ and utilizing the time derivative in equation (20) yields

$$\dot{\tilde{f}}_d = \dot{f}_d - \dot{\hat{f}}_d = \dot{f}_d - \dot{\varepsilon}_1 - \dot{\varepsilon}_2 = \dot{f}_d - \lambda\tilde{f}_d \tag{24}$$

where equations (17) and (19) have been used. Obviously, the observation error system (24), with $\dot{f}_d(t)$ viewed as an input, is input-to-state stable (ISS). By solving the differential equation (24), due to that $|\dot{f}_d| \le \upsilon_d$, the following results can be obtained

$$\begin{aligned}\tilde{f}_d(t) &= \tilde{f}_d(0)e^{-\lambda t} + e^{-\lambda t}\int_0^t \dot{f}_d(\tau)e^{\lambda\tau}\mathrm{d}\tau \\ &\le \tilde{f}_d(0)e^{-\lambda t} + e^{-\lambda t}\upsilon_d\int_0^t e^{\lambda\tau}\mathrm{d}\tau\end{aligned} \tag{25}$$

One can conclude from equation (25) that

$$\lim_{t\to\infty}\tilde{f}_d(t) \le \frac{\upsilon_d}{\lambda} \tag{26}$$

By performing similar analysis, we have

$$\lim_{t\to\infty}\tilde{f}_d(t) \ge -\frac{\upsilon_d}{\lambda} \tag{27}$$

Then, the conclusion $\lim_{t\to\infty}|\tilde{f}_d(t)| \le \frac{\upsilon_d}{\lambda}$ can be obtained. In addition, according to equation (24), one can obtain that

$$|\dot{\tilde{f}}_d(t)| \le |\dot{f}_d(t)| + |\lambda\tilde{f}_d(t)| \le 2\upsilon_d \tag{28}$$

The proof for this theorem is completed.

Controller design

Considering the control objectives of the underactuated crane system, the following sliding manifold is constructed

$$s = e_4(t) - e_4(0) - \int_0^t \varphi(\tau)\mathrm{d}\tau \tag{29}$$

where $\varphi(t)$ is defined as

$$\varphi = -c_4e_4 - c_3e_3 - c_2e_2 - c_1e_1 \tag{30}$$

where $c_1, c_2, c_3, c_4 \in \mathbb{R}^+$ are positive constants and selected to satisfy the subsequent conditions. Define that

$$A = \begin{bmatrix} 0 & 1 & 0 & 0 \\ 0 & 0 & 1 & 0 \\ 0 & 0 & 0 & 1 \\ -c_1 & -c_2 & -c_3 & -c_4 \end{bmatrix} \tag{31}$$

and assume that $\lambda(-A)$ is the real part of the leftmost eigenvalue of $-A$. c_1, c_2, c_3, c_4 should be chosen to make A Hurwitz and the upper bound of $\mu(e_3, e_4)$ in equation (16) $\varsigma < \lambda(-A)$. It can be observed from equation (29) that at $t = 0$

$$s(0) = e_4(0) - e_4(0) - \int_0^0 \varphi(\tau)\mathrm{d}\tau = 0 \tag{32}$$

which indicates that the initial states are on the sliding manifold $s(t)$.

Next, from the constructed sliding manifold equation (29), it is interesting to find out that one can construct the relation between the sliding manifold $s(t)$ and the auxiliary control input $f_u(t)$ by taking the derivative of $s(t)$ with respect to time. According to this characteristic, the following non-negative function is selected

$$V_s(t) = \frac{1}{2}s^2 \tag{33}$$

Taking the time derivative of $V_s(t)$ and making some algebraic manipulations, one can obtain that

$$\dot{V}_s(t) = s\left(f_u + f_d + f_f - \varphi\right) \tag{34}$$

where the time derivative of $s(t)$ in equation (29) and $\dot{e}_4(t)$ in equation (17) have been used. Then, in order to render the sliding manifold $s(t)$ attractive and invariant, based on the constructed disturbance observer in equations (20)–(22), the auxiliary control input $f_u(t)$ is designed as follows

$$f_u = -k_p\mathrm{sgn}(s)\sqrt{|s|} - k_i\int_0^t \mathrm{sgn}(s)\mathrm{d}\tau - \hat{f}_d - f_f + \varphi \tag{35}$$

where $\hat{f}_d(t)$ is the estimated disturbance in equations (20)–(22), $k_p, k_i \in \mathbb{R}^+$ are control parameters and chosen in light of the following criterions[49]

$$k_p = \omega\sqrt{\frac{4\nu\upsilon_d}{\kappa(1-\vartheta)}},\ k_i = \frac{2\upsilon_d(1+\vartheta)}{(1-\vartheta)} \tag{36}$$

where ω, ν, ϑ, κ meet the following conditions

$$\begin{aligned}&\omega - \frac{2}{\nu}\kappa > \kappa^2 - \vartheta(1+\omega)\kappa + \frac{1}{4}(1+\omega)^2 \\ &0 < \vartheta < 1,\ \nu > 1,\ \vartheta\nu > 1\end{aligned}$$

By substituting equation (35) into equation (3), and using equation (18), the ultimate control input $F(t)$ can be obtained

$$\begin{aligned}F = \frac{(M + m\sin^2\theta)l\cos\theta}{g}&\Big[-k_p\mathrm{sgn}(s)\sqrt{|s|} \\ &-k_i\int_0^t \mathrm{sgn}(s)\mathrm{d}\tau - \hat{f}_d - f_f + \varphi\Big] \\ &-ml\dot{\theta}^2\sin\theta - (M+m)g\tan\theta\end{aligned} \tag{37}$$

Stability analysis

Before proceeding to stability analysis, the following lemmas are introduced.

Lemma 1. For a system with the following dynamic equations

$$\begin{aligned}\dot{x}_1 &= -k_1\mathrm{sgn}(x_1)\sqrt{|x_1|} + x_2 \\ \dot{x}_2 &= -k_2\mathrm{sgn}(x_1) + \varrho_d\end{aligned} \tag{38}$$

If $\varrho_d \le L$ and k_1, k_2 satisfy the following conditions

$$k_1 = \omega\sqrt{\frac{2vL}{(1-\vartheta)\kappa}},\ k_2 = \frac{1+\vartheta}{1-\vartheta}L \tag{39}$$

where $L \in \mathbb{R}^+$ is a known parameter, and ω, v, ϑ, κ meet the following relationship

$$\omega - \frac{2}{v}\kappa > \kappa^2 - \vartheta(1+\omega)\kappa + \frac{1}{4}(1+\omega)^2$$
$$0 < \vartheta < 1,\ v > 1,\ \vartheta v > 1$$

Then, the states of the closed-loop system equation (38) will converge to the origin in finite time.[49]

Lemma 2. Consider a system with the following form

$$\begin{cases} \dot{x}_1 = x_2 \\ \dot{x}_2 = x_3 + d \\ \dot{x}_3 = x_4 \\ \dot{x}_4 = u \end{cases} \tag{40}$$

with the vanishing disturbance $d(t)$. Under the following control method

$$u = -c_4x_4 - c_3x_3 - c_2x_2 - c_1x_1 \tag{41}$$

and c_1, c_2, c_3, c_4 are chosen to satisfy that

$$A = \begin{bmatrix} 0 & 1 & 0 & 0 \\ 0 & 0 & 1 & 0 \\ 0 & 0 & 0 & 1 \\ -c_1 & -c_2 & -c_3 & -c_4 \end{bmatrix} \tag{42}$$

is Hurwitz. Assume that $\lambda(-A)$ is the real part of the leftmost eigenvalue of $-A$ and the upper bound of $d(t)$ is $\overline{d}$ ($\overline{d} \in \mathbb{R}^+$ is a priori known constant). If $\overline{d} < \lambda(-A)$, all states of the closed-loop system equation (40) will asymptotically converge to zero.[50]

Theorem 2. Under the control method equation (37) proposed here, the state variables $e_1(t)$, $e_2(t)$, $e_3(t)$, $e_4(t)$ always stay on the sliding manifold $s(t) = 0$ for $t \geq 0$.

Proof: Consider the sliding manifold in equation (29), the time derivative of which is

$$\dot{s}(t) = \dot{e}_4(t) - \varphi \tag{43}$$

By substituting equation (17) and the proposed auxiliary control input equation (35) into equation (43), the following equation can be obtained

$$\dot{s} = -k_p\mathrm{sgn}(s)\sqrt{|s|} - k_i\int_0^t \mathrm{sgn}(s)\mathrm{d}\tau + \tilde{f}_d \tag{44}$$

which can be rewritten as

$$\begin{aligned} \dot{s} &= -k_p\mathrm{sgn}(s)\sqrt{|s|} + \delta \\ \dot{\delta} &= -k_i\mathrm{sgn}(s) + \dot{\tilde{f}}_d \end{aligned} \tag{45}$$

where $\delta(t)$ is an auxiliary variable. Since the observation error system equation (24) is ISS, the observation error $\tilde{f}_d(t)$ will not escape to infinite. By employing the conclusion of Lemma 1, one can conclude that $s(t)$ and $\dot{s}(t)$ converge to zero in finite time. From equation (32), we know that the initial states are on the sliding manifold $s(t)$. Hence, it follows from the previous analysis that $s(t) = 0$ for $t \geq 0$. Thus, the proof is concluded.

Theorem 3. When the state variables stay on the sliding manifold, that is $s(t) = 0$, the state variables are bounded and converge to the equilibrium point in finite time, that is

$$\lim_{t\to\infty}[\ e_1\ \ e_2\ \ e_3\ \ e_4\ ]^{\mathrm{T}} = [\ 0\ \ 0\ \ 0\ \ 0\ ]^{\mathrm{T}} \tag{46}$$

Proof: According to the conclusion of Theorem 2, it is clear that $s(t) = 0$ and $\dot{s}(t) = 0$ for $t \geq 0$. Therefore, based on the equation (29), the following result can be obtained

$$\dot{s} = \dot{e}_4 + c_4e_4 + c_3e_3 + c_2e_2 + c_1e_1 = 0 \tag{47}$$

Then, the dynamic model equation (15) becomes

$$\begin{cases} \dot{e}_1 = e_2 \\ \dot{e}_2 = e_3 + \mu(e_3, e_4) \\ \dot{e}_3 = e_4 \\ \dot{e}_4 = -c_4e_4 - c_3e_3 - c_2e_2 - c_1e_1 \end{cases} \tag{48}$$

Since the control gains c_1, c_2, c_3, c_4 satisfy the conditions in Lemma 2. Hence, by invoking the conclusion of Lemma 2, all the states will converge to the equilibrium point finally, in the sense that

$$[\ e_1\ \ e_2\ \ e_3\ \ e_4\ ]^{\mathrm{T}} = [\ 0\ \ 0\ \ 0\ \ 0\ ]^{\mathrm{T}} \tag{49}$$

which is equivalent to

$$[\ x\ \ \dot{x}\ \ \theta\ \ \dot{\theta}\ ]^{\mathrm{T}} = [\ p_d\ \ 0\ \ 0\ \ 0\ ]^{\mathrm{T}} \tag{50}$$

Hereto, this completes the proof.

Remark 2. Existing robust control methods for underactuated crane systems usually assume that external disturbances satisfy the so-called matching condition, that is, the disturbances only exist in the same channel with the input. In addition, for these methods, the disturbances are removed by feedback control, which is a robust way.

Simulation Results

In this section, by use of the Matlab/Simulink software, two groups of simulation tests are made to demonstrate the excellent regulation and disturbance rejection characteristics of the devised control law in comparison with a previously proposed approach.[28] In the first group, assume that no disturbances exist in the overhead crane system, and the regulation performance of both methods is examined. In the second group, different disturbances consisting of the matched disturbance and unmatched disturbance are imposed on the crane system to examine the disturbance attenuation property of the developed approach. The expression of the selected energy-based regulation control (EBRC) method[28] is that

$$\begin{aligned} F = &-\frac{M + m\sin^2\theta}{1 + k_v + kk_v\cos\theta/l}\left[\frac{k_p}{\lambda}\tanh(x - k\sin\theta - p_d)\right. \\ &\left.+\frac{k_d}{\lambda}\left(\dot{x} - k\dot{\theta}\cos\theta\right) + \frac{kk_v}{\lambda}\sin\theta\left(g\cos\theta + l\dot{\theta}^2\right)/l\right] \\ &- m\sin\theta\left(g\cos\theta + l\dot{\theta}^2\right) \end{aligned} \tag{51}$$

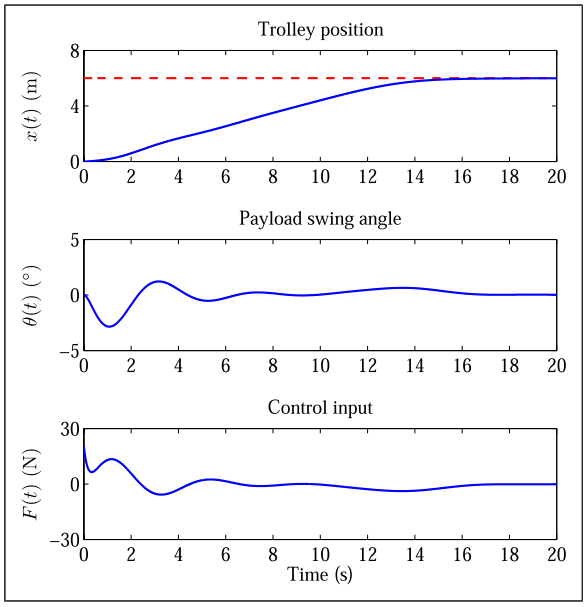

Figure 1. Simulation results of the EBRC method (equation (51)) (solid line: trolley displacement, payload swing angle, control variable; dashed line: the preset position).

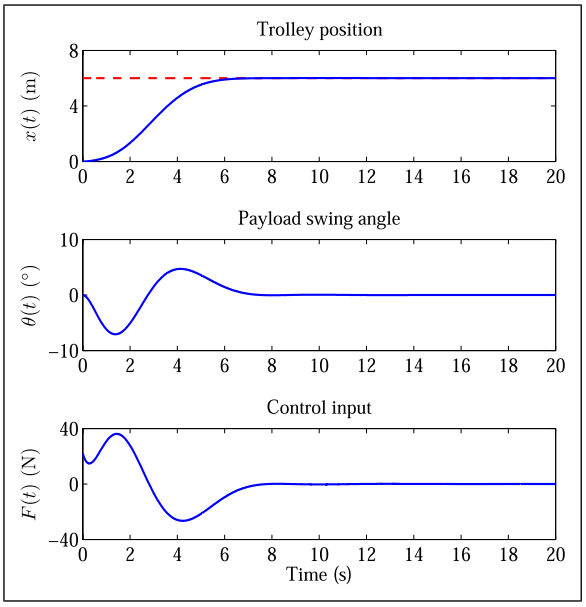

Figure 2. Simulation results of the proposed method (equation (37)) (solid line: trolley displacement, payload swing angle, control variable; dashed line: the preset position).

where p_d is the desired position. The control parameters of the EBRC method are set to be

$$k_p = 0.88,\ k_d = 1.88,\ k_v = 0.01,\ k = 3.2,\ \lambda = 1$$

and these parameters of the proposed approach are selected as

$$k_p = 6.32,\ k_i = 6,\ c_1 = 1, c_2 = 3.05,\ c_3 = 4,\ c_4 = 2.64$$

The observer gains of the designed disturbance observer are selected as

$$\lambda = 30,\ \alpha = 2$$

The system parameters of the overhead crane system are

$$M = 24\text{kg}, m = 12\text{kg}, l = 1.5\text{m}$$

The target location of the cart is chosen as p_d = 6 m.

Regulation Performance

The obtained simulation results of this test are given in Figures 1 and 2. In addition, with the aim of comparing the control performance of both methods quantitatively, quantified results are included in Table 1, which include the following specifications:

- Rise time t_r: The rise time is the first time that the cart reaches the preset location.
- Maximum payload swing angle $\theta_{\max}$: $\theta_{\max}$ is the maximum of the absolute value of the payload swing angle during the whole control process.
- Residual swing angle θ_{res}: Residual swing angle represents the maximum swing amplitude after the cart arrives at the preset location.
- Positioning error $e_{\max}$: Positioning error is the maximum error between the real position and the desired position after the cart arrives at the preset location.
- Maximum control input $F_{\max}$: $F_{\max}$ is the maximum control input that is required by the controller.

From the obtained simulation results in Figures 1 and 2, it can be seen that both the existing EBRC method and the developed method here could regulate the trolley to the target location and eliminate the payload oscillations in the end. Although the maximum payload swing angle under the EBRC method is smaller than the proposed control method, the maximum payload swing angle under the proposed control law here is acceptable. Moreover, by comparing the obtained specifications of the existing method and the designed method here, it can be seen that the existing EBRC approach takes much more time than the proposed approach to accomplish the control objectives. By contrast, the proposed control method shows better transient response and satisfactory steady state performance.

Robustness Performance

In this group, the payload mass is set to be m = 20 kg and the desired location of the trolley is set to be p_d = 4 m. In addition, to prove the strong robustness of the developed strategy against the matched and unmatched disturbances, the following disturbances are chosen

$$d_1(t) = 3\sin(0.4\pi t),\ d_2(t) = 2\cos(0.4\pi t)$$

The results of this test are depicted in Figures 3 and 4, respectively, and the corresponding quantified results are given in Table 1. From the simulation results of this group, one can find that even both matched and unmatched disturbances exist in the crane system, the cart is driven to the

Table 1. Quantified simulation results.

Controllers	t_r	θ_{max}	θ_{res}	e_{max}	F_{max}
Group 1: EBRC method (51)	**18.64**	2.85	0.03	0	20.48
Group 1: proposed method (37)	**7.05**	7.07	0.02	0	36.22
Group 2: EBRC method (51)	**12.81**	2.65	0.79	**0.05**	20.46
Group 2: proposed method (37)	**6.88**	4.68	0.03	0.01	28.98

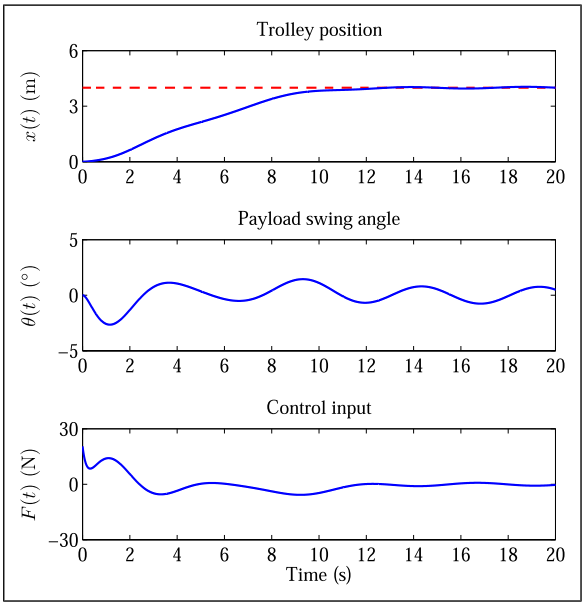

Figure 3. Simulation results of the EBRC method (equation (51)) (solid line: trolley displacement, payload swing angle, control variable; dashed line: the preset position).

preset location rapidly and accurately, and no residual payload oscillations exist under the proposed method, which shows superior disturbance estimation and compensation performance. By contrast, the rise time under the existing EBRC method is much longer than the proposed method. Moreover, there exist positioning error and residual payload oscillations under the EBRC method, and the efficiency of the crane system will be influenced.

Experimental examination

In this section, two groups of experimental tests are carried out in a laboratorial testbed (as shown in Figure 5) to further examine the regulation and disturbance rejection characteristics of the devised control approach. Similar to the simulation examination part, the existing EBRC method equation (51) is selected for a comparison study. The parameters of the testbed are

$$M = 9.473\text{kg}, m = 1\text{kg}, l = 0.55\text{m}$$

The control parameters of the existing EBRC approach equation (51) are

$$k_p = 0.156,\ k_d = 0.314,\ k_v = 1.4,\ k = 3.2,\ \lambda = 0.01$$

and these parameters of the proposed control method are

$$k_p = 2.35,\ k_i = 7.33,\ c_1 = 1, c_2 = 3,\ c_3 = 3,\ c_4 = 1.5$$

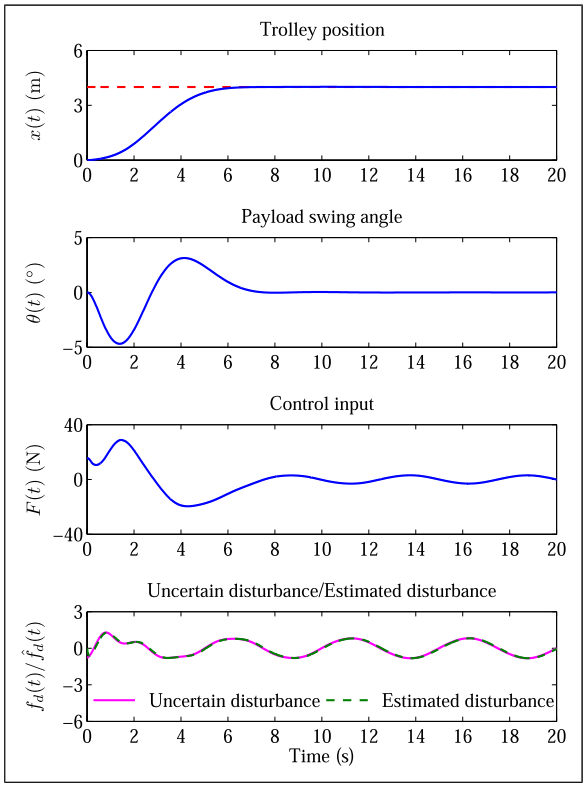

Figure 4. Simulation results of the proposed method (equation (37)) (The former three subfigures—*solid line:* trolley displacement, payload swing angle, control variable; *dashed line:* the preset position. The fourth subfigure—uncertain disturbance and estimated disturbance).

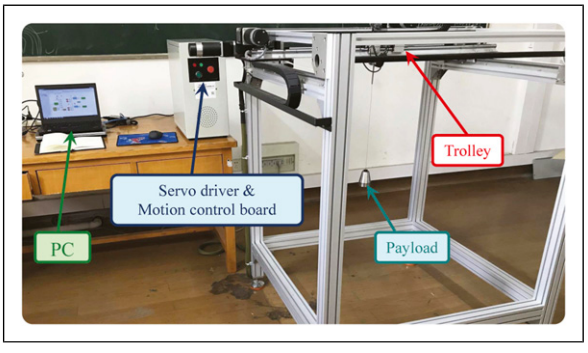

Figure 5. Experimental testbed.

The observer gains of the designed disturbance observer are selected as

$$\lambda = 10,\ \alpha = 2$$

The desired location of the cart is set to be $p_d = 0.4$ m.

Table 2. Quantified experimental results.

Controllers	t_r	θ_{max}	θ_{res}	e_{max}	F_{max}
Group 1: EBRC method (51)	**7.6**	1.65	0.04	0.002 2	12.47
Group 1: proposed method (37)	4.15	1.80	0.05	0.002 1	12.71
Group 2: EBRC method (51)	5.3	4.68	**0.44**	0.018	12.9
Group 2: proposed method (37)	3.96	4.91	0.13	0.015	14.63

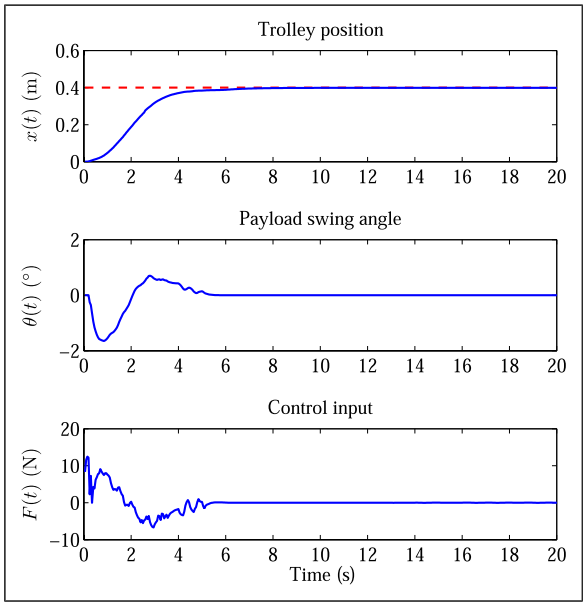

Figure 6. Experiment results of the EBRC method (equation (51)) (solid line: trolley displacement, payload swing angle, control variable; dashed line: the preset position).

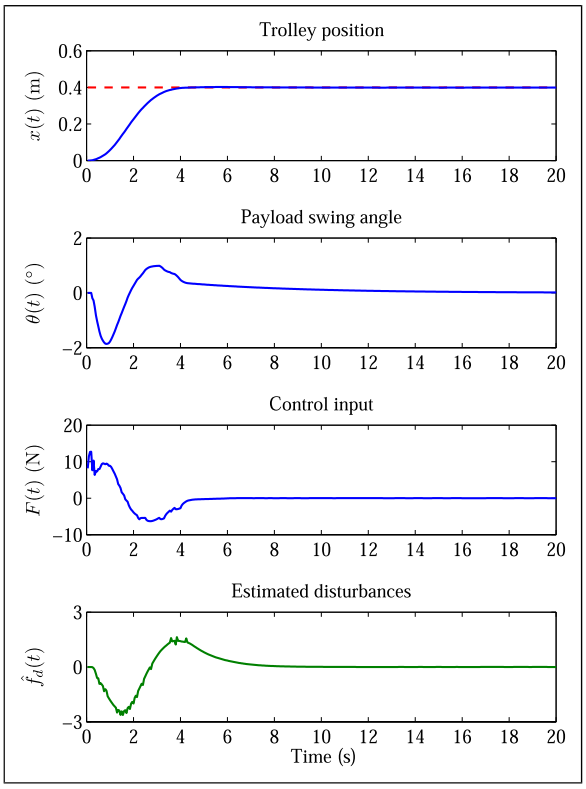

Figure 7. Experiment results of the proposed method (equation (37)) (The former three subfigures—*solid line:* trolley displacement, payload swing angle, control variable; *dashed line:* the preset position. The fourth subfigure—estimated disturbances).

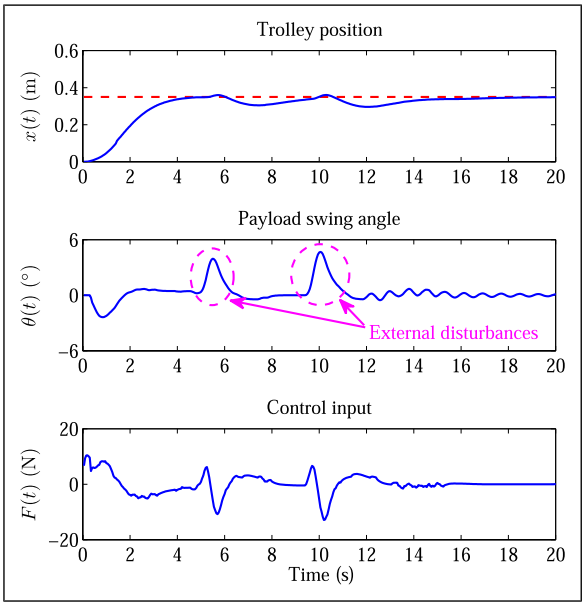

Figure 8. Experiment results of the EBRC method (equation (51)) (solid line: trolley displacement, payload swing angle, control variable; dashed line: the preset position).

Regulation Performance

The experimental results of this test are shown in Table 2, Figures 6 and 7. It can be observed from these results that both the existing EBRC method and the designed method here can drive the trolley to the target location accurately, suppress the payload oscillations effectively, and eliminate the residual payload oscillations finally. However, the comparative EBRC method takes 7.6 s to drive the trolley from the initial point to the preset location. By contrast, the rise time of the introduced approach here is only 4.15 s, which is more efficient than the existing EBRC method.

Robustness performance

In this test, the robustness of the devised approach will be examined. The target location of the trolley is set to be p_d = 0.35 m. In addition, uncertain disturbances are imposed on the payload during the control process. Hence, in the experimental test, the maximum payload swing angle is induced by the external disturbances.

The experimental results of this test are shown in Figures 8 and 9 and Table 2. From Figure 8, one can find that, under the existing EBRC method, the cart can be re-driven to the preset position when external disturbances disappear. However, the payload exist severe residual oscillations after the cart reaches the preset location. By contrast, for the proposed control approach, not only the trolley is re-driven

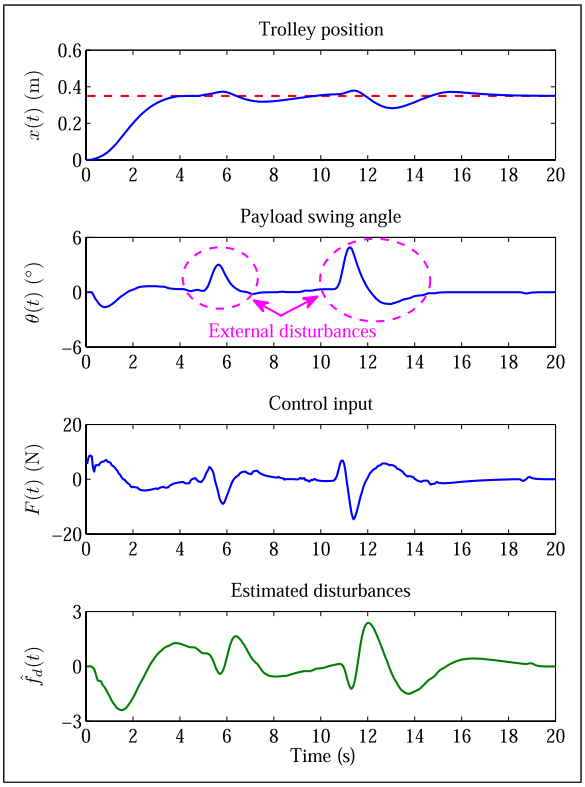

Figure 9. Experiment results of the proposed method (equation (37)) (The former three subfigures—*solid line:* trolley displacement, payload swing angle, control variable; *dashed line:* the preset position. The fourth subfigure—estimated disturbance).

to the preset location accurately, but also residual payload oscillations are removed even in the presence of uncertain disturbances, which is a benefit from the proposed disturbance observer and the global continuous sliding mode controller.

In summary, it is concluded that the designed control approach here exhibits satisfactory regulation control property and excellent robustness with respect to matched and unmatched disturbances.

Conclusion

In this paper, the regulation and disturbance rejection of the underactuated overhead crane system have been considered and a feedforward-control-based nonlinear control method is developed. The proposed control method consists of feedforward compensation control and continuous sliding mode control, which compensates uncertain disturbances and guarantees the convergence of the state variables. Compared with existing approaches for the overhead crane control, the designed control approach possesses both the theoretical and practical significance. On the one hand, both matched disturbances and unmatched disturbances are taken into account. On the other hand, the proposed control approach here is continuous and its robustness against disturbances is global. The included simulation and experimental results have shown that the strategy devised in this paper realizes the regulation control objective excellently and attenuates the effects of the matched and unmatched disturbances effectively. An important future work, adaptive sliding mode control without a priori bounded uncertainty[51] will be fully considered.

Declaration of conflicting interests

The author(s) declared no potential conflicts of interest with respect to the research, authorship, and/or publication of this article.

Funding

The author(s) disclosed receipt of the following financial support for the research, authorship, and/or publication of this article: This work was supported by the Zhejiang Science Technology Department Public Service Technology Research Project (grant number LGF20E070001); the Natural Science Foundation of Zhejiang Province (grant number LY22F030014); the National Natural Science Foundation of China (grant numbers 61 803 339).

ORCID iD

Xianqing Wu https://orcid.org/0000-0003-0623-6180

Note

1. Suppose that $d_2(t)$ vanishes at the origin and is locally Lipschitz.

References

1. Roy S and Baldi S. Towards structure-independent stabilization for uncertain underactuated Euler-Lagrange systems. *Automatica* 2020; 113: 108775.
2. Roy S, Baldi S and Ioannou PA. An adaptive control framework for underactuated switched Euler–Lagrange systems. *IEEE Trans Automatic Control* 2021: 1. DOI: 10.1109/TAC.2021.3108507.
3. Roy S, Baldi S, Li P, et al. Artificial-delay adaptive control for underactuated Euler–Lagrange robotics. *IEEE/ASME Trans Mechatronics* 2021; 26: 3064–3075. DOI: 10.1109/TMECH.2021.3052068.
4. Lu B, Fang Y, Sun N, et al. Antiswing control of offshore boom cranes with ship roll disturbances. *IEEE Trans Control Syst Technology* 2018; 26(2): 740–747.
5. Yang T, Sun N and Fang Y. Adaptive fuzzy control for a class of MIMO underactuated systems with plant uncertainties and actuator deadzones: Design and experiments. *IEEE Trans Cybernetics* 2021: 1–14. DOI: 10.1109/TCYB.2021.3050475.
6. Fu Y, Sun N, Yang T, et al. Adaptive coupling anti-swing tracking control of underactuated dual boom crane systems. *IEEE Trans Syst Man, Cybernetics: Syst* 2021: 1–13. DOI: 10.1109/TSMC.2021.3102244.
7. Liang X, Fang Y, Sun N, et al. Adaptive nonlinear hierarchical control for a rotorcraft transporting a cable-suspended payload. *IEEE Trans Syst Man, Cybernetics: Syst* 2021; 51(7): 4171–4182.
8. Wu X, Xu K, Ma M, et al. Output feedback control for an underactuated benchmark system with bounded torques. *Asian J Control* 2021; 23(3): 1466–1475.
9. Wu X, Zhao Y and Xu K. Nonlinear disturbance observer based sliding mode control for a benchmark system with uncertain disturbances. *ISA Trans* 2021; 110: 63–70.

10. Chen H and Sun N. An output feedback approach for regulation of 5-DOF offshore cranes with ship yaw and roll perturbations. *IEEE Trans Ind Electronics* 2022; 69: 1705–1716. DOI: 10.1109/TIE.2021.3055159.
11. Chen H, Fang Y and Sun N. An adaptive tracking control method with swing suppression for 4-DOF tower crane systems. *Mech Syst Signal Process* 2019; 123: 426–442.
12. Chen H and Sun N. Nonlinear control of underactuated systems subject to both actuated and unactuated state constraints with experimental verification. *IEEE Trans Ind Electronics* 2020; 67(9): 7702–7714.
13. Van Trieu P, Cuong HM, Dong HQ, et al. Adaptive fractional-order fast terminal sliding mode with fault-tolerant control for underactuated mechanical systems: Application to tower cranes. *Automation in Construction* 2021; 123: 103533.
14. Sorensen KL and Singhose WE. Command-induced vibration analysis using input shaping principles. *Automatica* 2008; 44(9): 2392–2397.
15. Masoud Z, Alhazza K, Abu-Nada E, et al. A hybrid command-shaper for double-pendulum overhead cranes. *J Vibration Control* 2012; 20(1): 24–37.
16. Maghsoudi MJ, Mohamed Z, Sudin S, et al. An improved input shaping design for an efficient sway control of a nonlinear 3D overhead crane with friction. *Mech Syst Signal Process* 2017; 92: 364–378.
17. Wu Z and Xia X. Optimal motion planning for overhead cranes. *IET Control Theor Appl* 2014; 8(17): 1833–1842.
18. Li F, Zhang C and Sun B. A minimum-time motion online planning method for underactuated overhead crane systems. *IEEE Access* 2019; 7: 54586–54594.
19. Wu X and He X. Enhanced damping-based anti-swing control method for underactuated overhead cranes. *IET Control Theor Appl* 2015; 9(12): 1893–1900.
20. Lu B, Fang Y and Sun N. Modeling and nonlinear coordination control for an underactuated dual overhead crane system. *Automatica* 2018; 91: 244–255.
21. Fatehi MH, Eghtesad M and Amjadifard R. Energy-based control of an underactuated crane system with a flexible cable and large swing angle. *Int J Curr Eng Technology* 2015; 5(3): 1727–1735.
22. Sun N, Fang Y and Zhang X. Energy coupling output feedback control of 4-DOF underactuated cranes with saturated inputs. *Automatica* 2013; 49(5): 1318–1325.
23. Sun N, Fang Y, Chen H, et al. Adaptive nonlinear crane control with load hoisting/lowering and unknown parameters: Design and experiments. *IEEE/ASME Trans Mechatronics* 2015; 20(5): 2107–2119.
24. Zhang M, Ma X, Rong X, et al. Adaptive tracking control for double-pendulum overhead cranes subject to tracking error limitation, parametric uncertainties and external disturbances. *Mech Syst Signal Process* 2016; 76-77: 15–32.
25. Sun N, Wu Y, Fang Y, et al. Nonlinear antiswing control for crane systems with double-pendulum swing effects and uncertain parameters: Design and experiments. *IEEE Trans Automation Sci Eng* 2018; 15(3): 1413–1422.
26. Gao J, Wang L, Gao R, et al. Adaptive control of uncertain underactuated cranes with a non-recursive control scheme. *J Franklin Inst* 2019; 356(18): 11305–11317.
27. Lu B, Fang Y and Sun N. Adaptive output-feedback control for dual overhead crane system with enhanced anti-swing performance. *IEEE Trans Control Syst Technology* 2020; 28(6): 2235–2248.
28. Wu X and He X. Nonlinear energy-based regulation control of three-dimensional overhead cranes. *IEEE Trans Automation Sci Eng* 2017; 14(2): 1297–1308.
29. Hamdy M, Shalaby R and Sallam M. A hybrid partial feedback linearization and deadbeat control scheme for a nonlinear gantry crane. *J Franklin Inst* 2018; 355(14): 6286–6299.
30. Wu X and He X. Partial feedback linearization control for 3-D underactuated overhead crane systems. *ISA Trans* 2016; 65: 361–370.
31. Wu Z, Xia X and Zhu B. Model predictive control for improving operational efficiency of overhead cranes. *Nonlinear Dyn* 2015; 79(4): 2639–2657.
32. Chen H, Fang Y and Sun N. A swing constraint guaranteed MPC algorithm for underactuated overhead cranes. *IEEE/ASME Trans Mechatronics* 2016; 21(5): 2543–2555.
33. Sun N, Yang T, Fang Y, et al. Transportation control of double-pendulum cranes with a nonlinear quasi-PID scheme: Design and experiments. *IEEE Trans Syst Man, Cybernetics: Syst* 2019; 49(7): 1408–1418.
34. Huang J, Liang Z and Zang Q. Dynamics and swing control of double-pendulum bridge cranes with distributed-mass beams. *Mech Syst Signal Process* 2015; 54-55: 357–366.
35. Cuong HM, Dong HQ, Trieu PV, et al. Adaptive fractional-order terminal sliding mode control of rubber-tired gantry cranes with uncertainties and unknown disturbances. *Mech Syst Signal Process* 2021; 154: 107601.
36. Almutairi NB and Zribi M. Sliding mode control of a three-dimensional overhead crane. *J Vibration Control* 2009; 15(11): 1679–1730.
37. Tuan LA, Lee S-G, Ko DH, et al. Combined control with sliding mode and partial feedback linearization for 3D overhead cranes. *Int J Robust Nonlinear Control* 2014; 24(18): 3372–3386.
38. Sun N, Fang Y and Chen H. A new antiswing control method for underactuated cranes with unmodeled uncertainties: Theoretical design and hardware experiments. *IEEE Trans Ind Electronics* 2015; 62(1): 453–465.
39. Zhang M, Zhang Y and Cheng X. Finite-time trajectory tracking control for overhead crane systems subject to unknown disturbances. *IEEE Access* 2019; 7: 55974–55982.
40. Ouyang H, Deng X, Xi H, et al. Novel robust controller design for load sway reduction in double-pendulum overhead cranes. *Proc Inst Mech Eng C: J Mech Eng Sci* 2019; 233(12): 4359–4371.
41. Zhang Z, Wu Y and Huang J. Differential-flatness-based finite-time anti-swing control of underactuated crane systems. *Nonlinear Dyn* 2017; 87(3): 1749–1761.
42. Vázquez C, Collado J and Fridman L. Super twisting control of a parametrically excited overhead crane. *J Franklin Inst* 2014; 351(4): 2283–2298.
43. Chwa D. Sliding-mode-control-based robust finite-time antisway tracking control of 3-D overhead cranes. *IEEE Trans Ind Electronics* 2017; 64(8): 6775–6784.
44. Zhang M, Zhang Y, Chen H, et al. Model-independent PD-SMC method with payload swing suppression for 3D overhead crane systems. *Mech Syst Signal Process* 2019; 129: 381–393.

45. Yang J, Li S and Yu X. Sliding-mode control for systems with mismatched uncertainties via a disturbance observer. *IEEE Trans Ind Electronics* 2013; 60(1): 160–169.
46. Li S, Sun H, Yang J, et al. Continuous finite-time output regulation for disturbed systems under mismatching condition. *IEEE Trans Automatic Control* 2015; 60(1): 277–282.
47. Liu Y, Guo F, He X, et al. Boundary control for an axially moving system with input restriction based on disturbance observers. *IEEE Trans Syst Man, Cybernetics: Syst* 2018; 49(11): 2242–2253.
48. Olfati-Saber R. *Nonlinear Control of Underactuated Mechanical Systems with Application to Robotics and Aerospace Vehicles*. Cambridge, MA, USA: PhD dissertation, Department of Electrical Engineering and Computure Science, Massachusetts Institue of Technology, 2001.
49. Moreno JA and Osorio M. Strict Lyapunov functions for the super-twisting algorithm. *IEEE Trans Automatic Control* 2012; 57(4): 1035–1040.
50. Xu R and Özgüner Ü. Sliding mode control of a class of underactuated systems. *Automatica* 2008; 44(1): 233–241.
51. Roy S, Baldi S and Fridman LM. On adaptive sliding mode control without a priori bounded uncertainty. *Automatica* 2020; 111: 108650.

TRANSACTIONS OF THE INSTITUTE OF MEASUREMENT & CONTROL

Article

Transactions of the Institute of Measurement and Control
2022, Vol. 44(10) 1960–1967

DOI: 10.1177/01423312211069107
journals.sagepub.com/home/tim
SAGE

Continuous sliding mode control for the translational oscillator with a rotating actuator system

Liqiang Wang[1], Xianqing Wu[2] and Meizhen Lei[2,3]

Abstract

The stabilization and disturbance rejection of the translational oscillator with a rotating actuator (TORA) are considered in this paper. To deal with the control issues, a novel continuous sliding mode control method is designed for the TORA system. Compared with existing sliding mode control methods for the TORA system, the proposed method here is continuous. Specifically, first, a global diffeomorphism is introduced for the model of the TORA system. Then, an elaborate sliding manifold is constructed, and a continuous sliding mode control scheme is developed to ensure the convergence of the sliding manifold. Furthermore, rigorous theoretical analysis is given. Finally, simulation tests are carried out, and the obtained simulation results demonstrate that the proposed method exhibits superior stabilization control performance and strong robustness.

Keywords

TORA, underactuated system, sliding mode control, Lyapunov theory

Introduction

The translational oscillator with a rotating actuator (TORA) system (as shown in Figure 1), including a translational cart and a rotating disk, is originally devised as a simplified model of a dual-spin spacecraft to investigate the resonance capture phenomenon (Bupp et al., 1998). Because of the special features of the TORA system, such as nonlinear, underactuated, strong coupling, and so forth, this system has been frequently utilized as an interesting benchmark example to examine the control performance of novel advanced control methodologies (Chen and Huang, 2012; Li et al., 2018, 2020; Mobayen, 2016; She et al., 2012; Wu et al., 2017; Zhang et al., 2016). In particular, as a classical nonlinear underactuated system, the TORA system is governed by fewer number of control inputs than controlled variables. Hence, the dynamics of the TORA system are much more complicated than these of full-actuated mechanical systems, and these characteristics bring about many challenges for the control design and make most existing control methodologies ineffective. Therefore, the control design issues of this system have attracted significant amount of interest.

During the past few decades, a lot of control methods have been reported for the TORA system in the literature. The existing methods mainly include two categories: cascade-based control and passivity-based control. For the former approach, the dynamics of the TORA system need to be reformulated by diffeomorphism or coordinate transformations. Specifically, Guo and Liu (2019) design a nonlinear controller on the basis of the backstepping technique. Assume that velocity variables are not available, many output feedback control approaches are reported (Gao et al., 2013; Wu et al., 2021a; Xu et al., 2020). On the basis of the passivity characteristic of the TORA system, some saturated constraint control schemes have been designed and published in the literature (Gao et al., 2014; Sun et al., 2017). Besides, taking uncertain disturbances or uncertain system parameters into consideration, other methodologies, including adaptive control (Wu et al., 2019; Wu and Gu, 2019), sliding mode control (Chen et al., 2018; Cheng et al., 2019; Mobayen, 2016; Wu et al., 2021b), intelligent control (Wu et al., 2018), and so forth (Liu et al., 2019; Tavakoli et al., 2005), have also been proposed and utilized to address the control issues of the underactuated TORA system.

So far, although a lot of control approaches have been investigated for the stabilization and disturbance attenuation of the TORA system, many issues need to be solved or require further improvements. For instance, existing control approaches, especially passivity-based control approaches (Gao et al., 2013; Sun et al., 2017; Wu et al., 2021a; Xu et al., 2020), only consider the stabilization control of this system, and they are usually designed based on an ideal model,

[1]Faculty of Mechanical and Automotive Engineering, Zhejiang University of Water Resources and Electric Power, China
[2]Faculty of Mechanical Engineering and Automation, Zhejiang Sci-Tech University, China
[3]Suzhou Industrial Technology Research Institute of Zhejiang University, China

Corresponding author:
Xianqing Wu, Faculty of Mechanical Engineering and Automation, Zhejiang Sci-Tech University, Hangzhou 310018, China.
Email: wxq@zstu.edu.cn

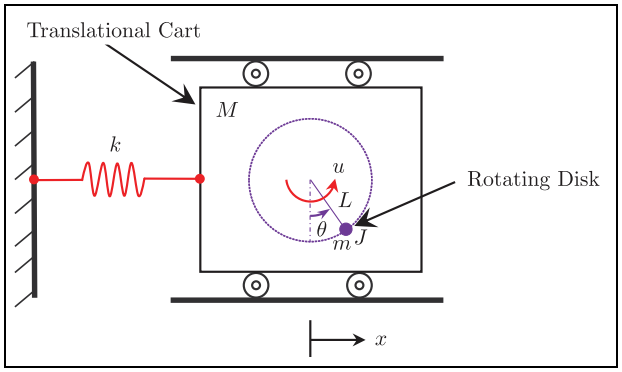

Figure 1. Schematic diagram of the TORA system.

without consideration for uncertain disturbances, unknown system parameters, unmodeled dynamics, and so on. However, uncertainties are unavoidable for practical mechanical systems. In addition, uncertain disturbances can be addressed by sliding-mode-based control schemes (Chen et al., 2018; Cheng et al., 2019; Mobayen, 2016; Wu et al., 2018), but these existing methods are discontinuous, which will result in severe chattering problems and even may cause potential damages to actuating devices.

To attenuate and eliminate the effects of disturbances, sliding mode control has been proven to be an effective approach, which has been widely investigated and utilized in many areas. Therefore, motivated to overcome the existing drawbacks of reported control methods, a continuous sliding mode controller is exploited for the control design issue of the TORA system here. In particular, a change of coordinates in original dynamics is made. Subsequently, an elaborate sliding manifold is introduced, and a continuous sliding mode controller is devised. The corresponding convergence result of all the states is proven via rigorous theoretical analysis. Finally, some simulation tests are provided to verify the stabilization performance and robustness of the introduced continuous sliding mode controller. In sum, the proposed controller here possesses the following features:

1. An elaborate sliding manifold is introduced, based on which a continuous sliding mode controller is developed for the TORA system.
2. In comparison with traditional sliding mode control approaches, the proposed sliding mode controller is continuous, which is convenient for engineering implementations.

The remainder of the paper is organized as follows. In the "System model" section, the dynamic equations of the TORA system are provided, and a change of coordinates in original dynamics is made. In the "Main results" section, an elaborate sliding manifold is constructed, a corresponding continuous sliding mode controller is developed, and the detailed stability analysis is given. In the "Simulation verification" section, the stabilization performance and robustness of the proposed control method are verified through numerical simulation tests. Finally, the main work of this paper is summarized in the "Conclusion" section.

System model

The schematic diagram of the TORA system is shown in Figure 1. It consists of a translational cart with mass M connected to one fixed end through a linear spring with spring constant k. On the cart, a rotating disk is actuated by a direct current (DC) motor with the control torque $u(t)$. The mass of the disk is m, and the distance between the disk and the rotational axis is L. The rotating disk has moment of inertia J around its center of mass. The dynamics of the TORA system can be obtained by using Newton's law as follows

$$(M+m)\ddot{x} + mL\left(\ddot{\theta}\cos\theta - \dot{\theta}^2\sin\theta\right) + kx = 0 \tag{1}$$

$$mL\ddot{x}\cos\theta + \left(mL^2 + J\right)\ddot{\theta} = u + d \tag{2}$$

where $x(t)$ is the displacement of the translational cart, $\theta(t)$ denotes the angular position of the disk, and $d(t)$ represents the lumped disturbances/uncertainties.

Before proceeding with the control development, a global diffeomorphism is introduced

$$\eta_1 = \theta, \eta_2 = x, \eta_3 = \dot{x} + \frac{mL\dot{\theta}\cos\theta}{M+m}, \vartheta = \dot{\theta} \tag{3}$$

which transforms the dynamics (equations (1) and (2)) into the following form

$$\dot{\eta}_1 = \vartheta \tag{4a}$$

$$\dot{\eta}_2 = -\frac{mL\vartheta\cos\eta_1}{M+m} + \eta_3 \tag{4b}$$

$$\dot{\eta}_3 = -\frac{k\eta_2}{M+m} \tag{4c}$$

$$\dot{\vartheta} = u_a + d_e + \Pi \tag{4d}$$

where $u_a(t)$ is an auxiliary control variable to be designed, $d_e(t)$ is the equivalent external disturbance term, and $\Pi(t)$ is an auxiliary function, the expressions of which are

$$u_a = \frac{M+m}{(M+m)(mL^2+J) - m^2L^2\cos^2\eta_1}u \tag{5}$$

$$d_e = \frac{M+m}{(M+m)(mL^2+J) - m^2L^2\cos^2\eta_1}d \tag{6}$$

$$\Pi = \frac{-mL\cos\eta_1\left(mL\vartheta^2\sin\eta_1 - k\eta_2\right)}{(M+m)(mL^2+J) - m^2L^2\cos^2\eta_1} \tag{7}$$

Considering real-world mechanical systems, suppose that the time derivative of $d_e(t)$ satisfies the following condition

$$|\dot{d}_e(t)| \leq \varpi \tag{8}$$

where $\varpi \in \mathbb{R}^+$ is a prior known positive constant.

The aim of this paper is to maintain the system at the equilibrium point using an appropriate controller, that is

$$\lim_{t\to\infty}[x \quad \dot{x} \quad \theta \quad \dot{\theta}]^{\mathrm{T}} = [0 \quad 0 \quad 0 \quad 0]^{\mathrm{T}} \tag{9}$$

Based on the introduced global diffeomorphism (equation (3)), it is easy to see that equation (9) is equivalent to

$$\lim_{t\to\infty}[\eta_1 \quad \eta_2 \quad \eta_3 \quad \vartheta]^{\mathrm{T}} = [0 \quad 0 \quad 0 \quad 0]^{\mathrm{T}} \tag{10}$$

Hence, the new dynamics (equation (4)) will be utilized for the forthcoming control design and stability analysis.

Remark 1: The stabilization and disturbance rejection of the TORA system are more complex than it might appear at first glance. On one hand, the nonlinear coupling between the rotational motions and the translational oscillations increases the difficulty of the control design. On the other hand, it is very challenging to construct a suitable sliding manifold which can simultaneously stabilize both actuated and unactuated system states.

Main results

In this section, the detailed control design process and stability analysis will be provided.

Control design

First, based on the dynamics (equation (4)), a sliding manifold is constructed as follows

$$s = \vartheta + k_1\eta_1 - k_2\eta_2\cos\eta_1 \tag{11}$$

where $k_1, k_2 \in \mathbb{R}^+$ are positive constants. Taking the time derivative of both sides of equation (11), the following equation can be obtained

$$\dot{s} = \dot{\vartheta} + k_1\vartheta + k_2\left(\frac{mL\vartheta\cos\eta_1}{M+m} - \eta_3\right)\cos\eta_1 + k_2\eta_2\vartheta\sin\eta_1 \tag{12}$$

Then, based on equalities (4d) and (12), the auxiliary control variable $u_a(t)$ is designed as follows

$$\begin{aligned} u_a = & -k_p\sqrt{|s|}\mathrm{sign}(s) - k_i\int_0^t \mathrm{sign}(s)\mathrm{d}\tau - \Pi \\ & - k_1\vartheta - k_2\left(\frac{mL\vartheta\cos\eta_1}{M+m} - \eta_3\right)\cos\eta_1 - k_2\eta_2\vartheta\sin\eta_1 \end{aligned} \tag{13}$$

where $k_p, k_i \in \mathbb{R}^+$ are positive constants and chosen as follows (Moreno and Osorio, 2012)

$$k_p = \alpha\sqrt{\frac{2\nu\varpi}{(1-\beta)\gamma}}, \quad k_i = \frac{1+\beta}{1-\beta}\varpi \tag{14}$$

To guarantee the robustness, finite-time stability of the sliding mode control method, $\alpha, \beta, \gamma, \nu$ should satisfy the following conditions (Moreno and Osorio, 2012)

$$\begin{aligned} & \alpha - \frac{2}{\nu}\gamma > \gamma^2 - \beta(1+\alpha)\gamma + \frac{1}{4}(1+\alpha)^2 \\ & 0 < \beta < 1, \nu > 1, \beta\nu > 1 \end{aligned}$$

Thus, based on equation (5), the actual control variable applied to the TORA system is yielded

$$u = \frac{(M+m)(mL^2+J) - m^2L^2\cos^2\eta_1}{M+m}u_a \tag{15}$$

where the expression of $u_a(t)$ is provided in equation (13).

Stability analysis

In order to prove the performance of the proposed continuous sliding mode controller, the following theorem is given and the corresponding theoretical analysis is provided.

Theorem 1: Under the control of the proposed continuous sliding mode controller (equation (15)), the control objective can be achieved, that is

$$\lim_{t\to\infty}\left[x \quad \dot{x} \quad \theta \quad \dot{\theta}\right]^{\mathrm{T}} = [0 \quad 0 \quad 0 \quad 0]^{\mathrm{T}} \tag{16}$$

Proof: First, by substituting equations (4d) into (12) for $\dot{\vartheta}(t)$, the following equation can be obtained

$$\dot{s} = -k_p\sqrt{|s|}\mathrm{sign}(s) - k_i\int_0^t \mathrm{sign}(s)\mathrm{d}\tau + d_e \tag{17}$$

where the designed auxiliary control variable $u_a(t)$ in equation (13) has been used. Then, by introducing an auxiliary variable, equation (17) can be rewritten in the following form

$$\begin{cases} \dot{s} = -k_p\sqrt{|s|}\mathrm{sign}(s) + \phi \\ \dot{\phi} = -k_i\mathrm{sign}(s) + \dot{d}_e \end{cases} \tag{18}$$

Since the control constants k_p, k_i satisfy the conditions given in equation (14), by employing Theorem 2 of Moreno and Osorio (2012), we can conclude that

$$s \to 0, \dot{s} \to 0 \tag{19}$$

in finite time T_f. According to the expression of $s(t)$ in equation (11), it is clear that

$$s = 0 \Leftrightarrow \vartheta = -k_1\eta_1 + k_2\eta_2\cos\eta_1 \tag{20}$$

after finite time T_f.

Next, in order to analyze the convergence of all the states of the closed-loop system, consider a Lyapunov function candidate with the following form

$$V_\eta(t) = \frac{k_1}{2}\eta_1^2 + \frac{k_2(M+m)}{2mL}\eta_2^2 + \frac{k_2(M+m)^2}{2mLk}\eta_3^2 \quad (21)$$

Differentiating both sides of equation (21) with respect to time yields that

$$\dot{V}_\eta(t) = -\vartheta(-k_1\eta_1 + k_2\eta_2\cos\eta_1) \quad (22)$$

where the global diffeomorphism (equation (3)) and the dynamics (equation (4)) have been utilized. On the basis of the previous conclusion (equation (20)), it can be yielded that

$$\dot{V}_\eta(t) = -\vartheta^2 = -(-k_1\eta_1 + k_2\eta_2\cos\eta_1)^2 \quad (23)$$

after finite time T_f, which indicates that the Lyapunov function candidate $V_\eta(t)$ is nonincreasing. To examine the convergence of the Lyapunov function candidate $V_\eta(t)$, let

$$\mathcal{S} = \{(\eta_1, \eta_2, \eta_3) | \dot{V}_\eta(t) = 0\} \quad (24)$$

It is clear from equations (23) and (24) that in $\mathcal{S}$

$$\vartheta = 0, k_1\eta_1 - k_2\eta_2\cos\eta_1 = 0 \Rightarrow \dot{\vartheta} = 0 \quad (25)$$

which, together with equations (4a) and (4b), imply that

$$\eta_1 = c_1, \eta_2 = c_2 \Rightarrow \dot{\eta}_2 = \eta_3 = 0 \quad (26)$$

which, together with equation (4c), further indicate that

$$\eta_2 = 0 \quad (27)$$

where $c_1, c_2 \in \mathbb{R}$ are constants. On the basis of the previous conclusion $\eta_2 = 0$ and equation (25), one can conclude that

$$\eta_1 = 0 \quad (28)$$

Hence, from the previous analysis, one can find that the only solution that can stay identically in $\mathcal{S}$ is the equilibrium point. Hence, by applying LaSalle's invariant principle (Khalil, 2002), we can conclude that the origin is asymptotically stable. This completes the proof.

Simulation verification

In this section, the performance of the proposed continuous sliding mode controller will be verified by use of MATLAB/Simulink. Specifically, two groups of simulation tests will be given to verify the superior performance of the developed scheme. More precisely, in the first group, the stabilization control performance of the proposed continuous sliding mode control method is examined. In the second group, the robustness of the proposed continuous sliding mode controller under different uncertain disturbances will be verified. In order to show the stronger robustness of the developed control scheme, the adaptive control (adaptive control (ADC)) method of Wu and Gu (2019) is chosen for a comparison study. The expression of the ADC approach is

$$u = -\frac{k_p\theta + k_d\dot{\theta} + k_v x\cos\theta\hat{\omega}}{1+k_v} - \frac{k_c\theta}{(k_b^2 - \theta^2)(1+k_v)} \quad (29)$$

where $k_p, k_d, k_c \in \mathbb{R}^+$ stand for control parameters, k_b is the state constraint parameter, and $\hat{\omega}$ is the estimated value of ω, which is generated by the following equation

$$\dot{\hat{\omega}} = \mathrm{Proj}(\hat{\omega}, \psi) \quad (30)$$

where $\psi = k_u x\dot{\theta}\cos\theta$ and $k_u \in \mathbb{R}^+$ is an update gain. For brevity, the detailed expression of the update mechanism is omitted here. The values of the control parameters of the ADC method are selected as the same as those given in Wu and Gu (2019).

For the subsequent simulation studies, the system parameters of the TORA system are chosen to be (Wu and Gu, 2019)

$$M = 1.3608\,\mathrm{kg}, m = 0.096\,\mathrm{kg}, k = 186.3\,\mathrm{N/m} \quad (31)$$

$$L = 0.0592\,\mathrm{m}, J = 0.0002175\,\mathrm{kg}\cdot\mathrm{m}^2 \quad (32)$$

According to the conditions given in equation (14) and after abundant simulation tests, the control parameters of the proposed continuous sliding mode controller are set as follows

$$k_p = 42.42, k_i = 38, k_1 = 11, k_2 = 650$$

Stabilization control examination

In this group, different initial conditions will be considered and corresponding simulation results will be provided. Toward this end, the following two cases are examined:

Case 1: $[x(0)\dot{x}(0)\theta(0)\dot{\theta}(0)]^{\mathrm{T}} = [-0.02\,\mathrm{m}\ \ 0\ \ 0.3\,\mathrm{rad}\ \ 0]^{\mathrm{T}}$.
Case 2: $[x(0)\dot{x}(0)\theta(0)\dot{\theta}(0)]^{\mathrm{T}} = [\ \ 0.02\,\mathrm{m}\ \ 0\ \ 0\ \ 0]^{\mathrm{T}}$.

Figures 2–5 record the simulation results of the abovementioned two cases, respectively. It can be found from Figures 2–5 that the state responses of both cases are stabilized to the equilibrium point and there are no residual oscillations for the translational cart, which indicates that both the ADC method (equation (29)) and the designed method (equation (15)) can guarantee that the cart and the disk are driven to the original point even for different initial conditions. Furthermore, from the control input curves in Figures 3 and 5, one can find that the developed sliding mode controller is continuous, which is of important significance for practical applications.

Robustness to uncertain disturbances

In this part, the robustness of the proposed continuous sliding control scheme against different external disturbances will be verified. To this end, pulse disturbance, random disturbance, and sine disturbance are imposed on the TORA system. For the following two cases, we assume that the initial states are zeros.

Case 1: The different disturbances are $d(t) = 0$ for $t < 5$ s and $d(t) = 0.08$ for $5\,\mathrm{s} \leqslant t < 5.2$ s; random disturbance with

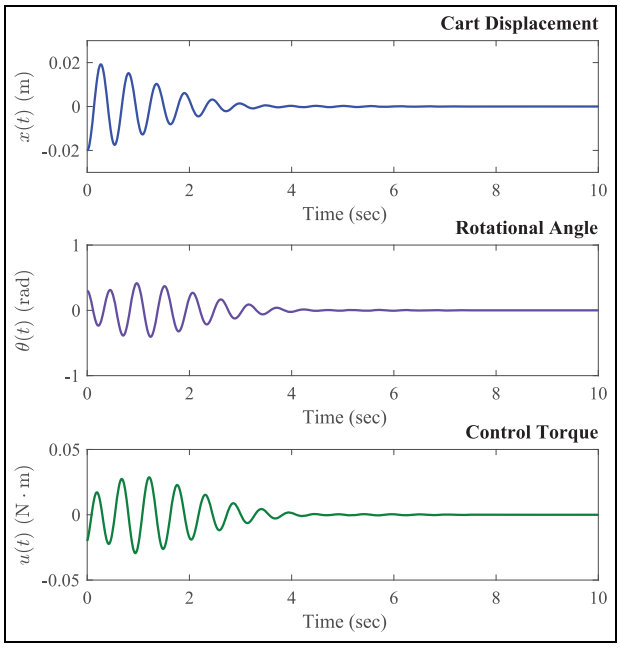

Figure 2. Simulation results of stabilization examination, Case 1: the existing method (equation (29)).

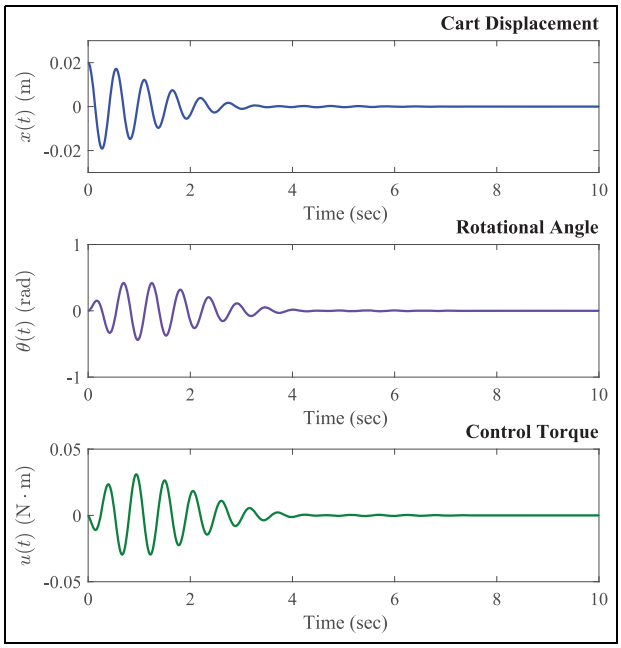

Figure 4. Simulation results of stabilization examination, Case 2: the existing method (equation (29)).

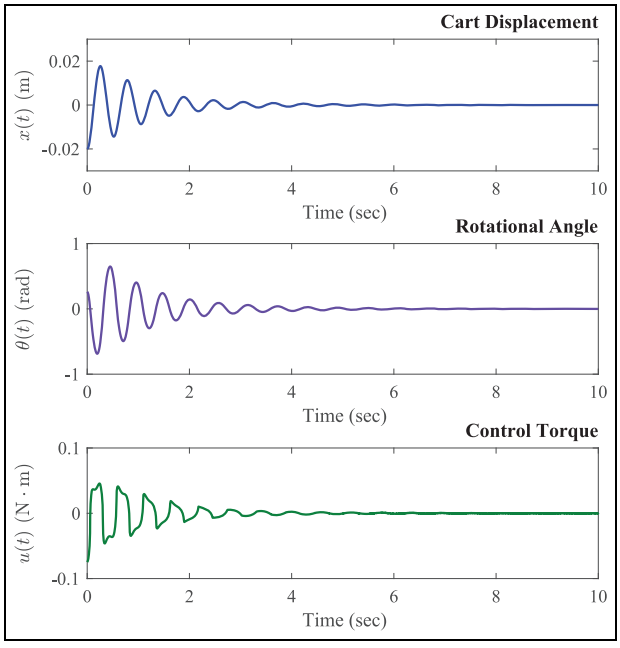

Figure 3. Simulation results of stabilization control examination, Case 1: the proposed method (equation (15)).

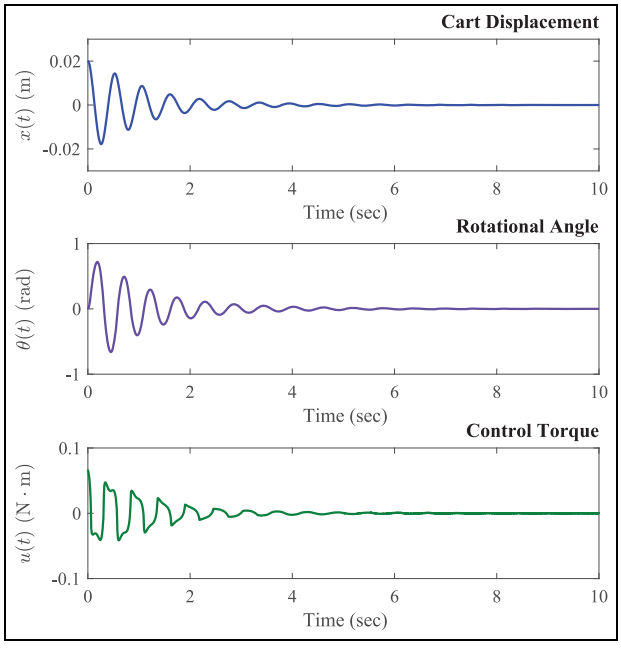

Figure 5. Simulation results of stabilization control examination, Case 2: the proposed method (equation (15)).

the amplitude 0.08 for $20\,\text{s} \leqslant t < 30\,\text{s}$ and $d(t) = 0$ for $30\,\text{s} \leqslant t \leqslant 40\,\text{s}$.

Case 2: The disturbance is $d(t) = 0.5\sin(0.2\pi t)/(1 + t)$ for $0 \leqslant t \leqslant 40\,\text{s}$.

For the above two cases, the obtained results are plotted in Figures 6–9. Since uncertain disturbances are neglected when making control design for the existing control method

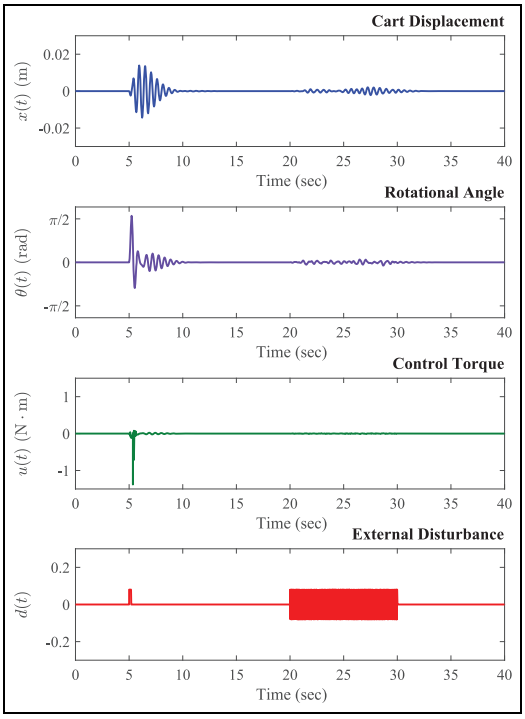

Figure 6. Simulation results of robustness examination, Case 1: the existing method (equation (29)).

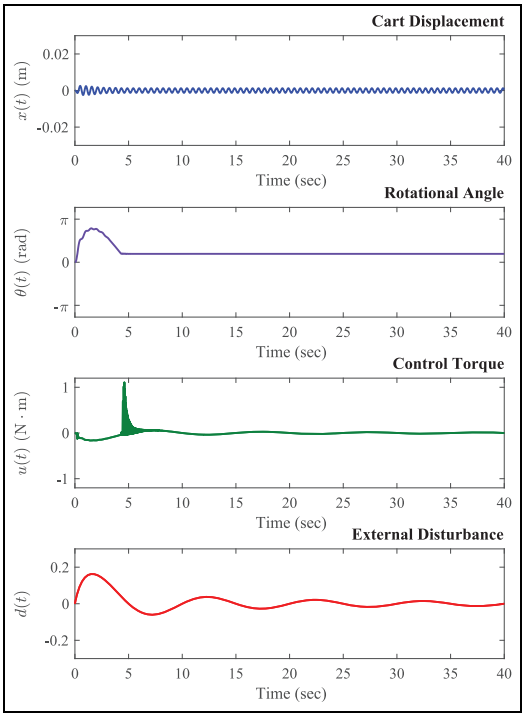

Figure 8. Simulation results of robustness examination, Case 2: the existing method (equation (29)).

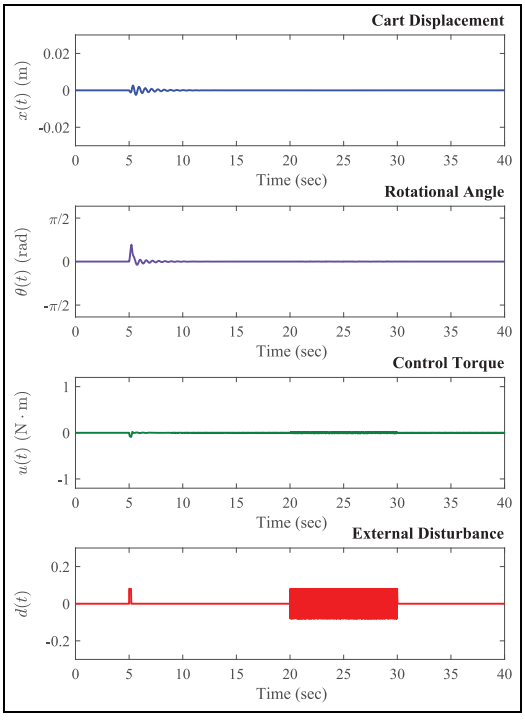

Figure 7. Simulation results of robustness examination, Case 1: the proposed method (equation (15)).

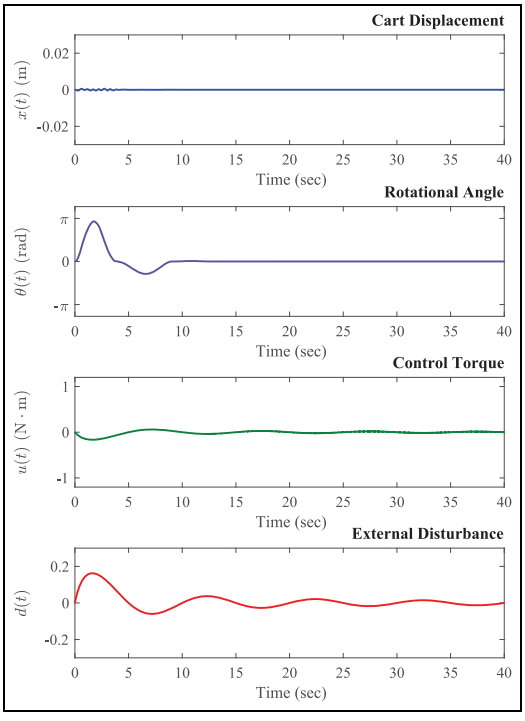

Figure 9. Simulation results of robustness examination, Case 2: the proposed method (equation (15)).

(equation (29)), it can be seen from the obtained simulation results for the existing control method (equation (29)) in Figures 6 and 8 that the effects of external disturbances cannot be eliminated by the ADC method (equation (29)), especially the rotating disk is not stabilized to the original point in Case 2. In addition, the ADC method (equation (29)) exhibits the control peaking phenomenon, which could destabilize the system. On the contrary, uncertain disturbances are taken into account in this paper; the stabilization performance of the developed method is hardly affected by different uncertain disturbances. The results of this group indicate that the developed continuous sliding mode control method shows superior disturbance rejection performance.

Remark 2: From the simulation results obtained in the above two groups of simulation tests, it can be found that the stabilization performance of the two methods is similar when there are no uncertain disturbances for the TORA system. But the disturbance rejection performance of the existing method (equation (29)) is unsatisfactory because of the presence of uncertain disturbances. On the contrary, even in the presence of uncertain disturbances, the control performances of the proposed method are satisfactory.

Conclusion

In this paper, a continuous sliding mode controller has been proposed for the stabilization and disturbance rejection of the TORA system. The proposed method exhibits excellent stabilization and disturbance rejection performance. On one hand, uncertain disturbances can be eliminated by the proposed control method. On the other hand, compared with traditional sliding mode controllers, the proposed sliding mode controller is continuous. The simulation results have shown that the proposed continuous sliding mode controller possesses superior stabilization and disturbance elimination performance.

Declaration of conflicting interests

The author(s) declared no potential conflicts of interest with respect to the research, authorship, and/or publication of this article.

Funding

The author(s) disclosed receipt of the following financial support for the research, authorship, and/or publication of this article: This work was supported by the Zhejiang Science Technology Department Public Service Technology Research Project (grant number LGF20E070001), the Natural Science Foundation of Zhejiang Province (grant number LY22F0 30014), and the National Natural Science Foundation of China (grant number 61803339).

ORCID iD

Xianqing Wu https://orcid.org/0000-0003-0623-6180

References

Bupp RT, Bernstein DS and Coppola VT (1998) A benchmark problem for nonlinear control design. *International Journal of Robust Nonlinear Control 8(4–5):* 307–310.

Chen YF and Huang AC (2012) Controller design for a class of underactuated mechanical systems. *IET Control Theory and Applications* 6(1): 103–110.

Chen Z, Wu X, Ou X, et al. (2018) Sliding mode control of the RTAC system. In: *Proceedings of the 2018 IEEE 7th data driven control and learning systems conference*, Enshi, China, 25–27 May, pp. 682–687. New York: IEEE.

Cheng K, Zhang Y, Li L, et al. (2019) Adaptive sliding mode control of inclined TORA system. In: *Proceedings of the 2019 Chinese control conference, Guangzhou*, China, 27–30 July, pp. 797–802. New York: IEEE.

Gao B, Bao Y, Xie J, et al. (2014) Passivity-based control of two-dimensional translational oscillator with rotational actuator. *Transactions of the Institute of Measurement and Control* 36(1): 111–118.

Gao B, Xu J, Zhao J, et al. (2013) Stabilizing control of an underactuated 2-dimensional TORA with only rotor angle measurement. *Asian Journal of Control* 15(5): 1477–1488.

Guo W and Liu D (2019) Nonlinear dynamic surface control for the underactuated translational oscillator with rotating actuator system. *IEEE Access* 7: 11844–11853.

Khalil HK (2002) *Nonlinear Systems* (3rd edn). Upper Saddle River, NJ: Prentice Hall.

Li J, Li J, Wu Z, et al. (2020) Practical tracking control with prescribed transient performance for Euler-Lagrange equation. *Journal of the Franklin Institute* 357(10): 5809–5830.

Li W, Liu L and Feng G (2018) Cooperative control of multiple nonlinear benchmark systems perturbed by second-order moment processes. *IEEE Transactions on Cybernetics* 50(3): 902–910.

Liu C, Gao B, Zhao J, et al. (2019) Orbitally stabilizing control for the underactuated translational oscillator with rotational actuator system: Design and experimentation. *Proceedings of the Institution of Mechanical Engineers, Part I: Journal of Systems and Control Engineering* 233(5): 491–500.

Mobayen S (2016) A novel global sliding mode control based on exponential reaching law for a class of underactuated systems with external disturbances. *Journal of Computational and Nonlinear Dynamics* 11(2): 021011–021011.

Moreno JA and Osorio M (2012) Strict Lyapunov functions for the super-twisting algorithm. *IEEE Transactions on Automatic Control* 57(4): 1035–1040.

She J, Zhang A, Lai X, et al. (2012) Global stabilization of 2-DOF underactuated mechanical systems: An equivalent-input-disturbance approach. *Nonlinear Dynamics* 69(1): 495–509.

Sun N, Wu Y, Fang Y, et al. (2017) Nonlinear stabilization control of multiple-RTAC systems subject to amplitude-restricted actuating torques using only angular position feedback. *IEEE Transactions on Industrial Electronics* 64(4): 3084–3094.

Tavakoli M, Taghirad HD and Abrishamchian M (2005) Identification and robust H∞ control of the rotational/translational actuator system. *International Journal of Control, Automation, and Systems* 3(3): 387–396.

Wu T, Gui W, Hu D, et al. (2018) Adaptive fuzzy sliding mode control for translational oscillator with rotating actuator: A fuzzy model. *IEEE Access* 6: 55861–55869.

Wu X and Gu M (2019) Adaptive control of the TORA system with partial state constraint. *Transactions of the Institute of Measurement and Control* 41(4): 1172–1177.

Wu X, Xu K, Ma M, et al. (2021a) Output feedback control for an underactuated benchmark system with bounded torques. *Asian Journal of Control* 23(3): 1466–1475.

Wu X, Zhao Y and Xu K (2021b) Nonlinear disturbance observer based sliding mode control for a benchmark system with uncertain disturbances. *ISA Transactions* 110: 63–70.

Wu Y, Sun N and Fang Y (2019) An increased nonlinear coupling motion controller for underactuated multi-TORA systems: Theoretical design and hardware experimentation. *IEEE Transactions on Systems, Man, and Cybernetics: Systems* 49(6): 1186–1193.

Wu Z, Wang S and Cui M (2017) Tracking controller design for random nonlinear benchmark system. *Journal of the Franklin Institute* 354(1): 360–371.

Xu K, Wu X, Ma M, et al. (2020) Energy-based output feedback control of the underactuated 2DTORA system with saturated inputs. *Transactions of the Institute of Measurement and Control* 42(14): 2822–2829.

Zhang X, Huang X, Lu H, et al. (2016) Forwarding-based immersion and invariance control for η-dimensional strict-feedback nonlinear systems. *Nonlinear Dynamics 83(1–2):* 483–496.

Novel phase-locked loop-based resonant frequency tracking control for linear reciprocating compressor

Liqiang Wang[1], Xiaofan Yu[2], Meizhen Lei[3,*] and Xiuxing Yin[3]
[1]*Faculty of Mechanical and Automotive Engineering, Zhejiang University of Water Resources and Electric Power, 2nd Street, Hangzhou 310018, China;* [2]*Research and Development Center, Hangzhou NetEase Cloud Music Technology Co., Ltd., Jianghong Road, Hangzhou 310052, China;* [3]*Faculty of Mechanical Engineering and Automation, Zhejiang Sci-Tech University, 2nd Street, Hangzhou 310018, China*

Abstract

The paper presents a novel phase-locked loop (PLL)-based resonant frequency tracking method for linear compressors with oscillatory motions. The proposed method achieves the phase-locked control between two signals by using PLL, which includes a multiplier, and a low-pass filter to obtain the phase signal difference. Consequently, based on the phase signal difference, the electrical frequency of the power supply can be adjusted through a PI (proportional-derivative) regulator such that the phase signal difference converges to 90° and the linear compressor works under the resonant frequency conditions. The analytical expression of the resonant frequency condition is proposed for the linear compressor. Then, the detailed design and procedure of the proposed method are presented. The designed method and the resonant frequency characteristics are verified by using the simulation experiment. The simulated results demonstrate that the proposed algorithm has faster response speed and higher convergence accuracy to step load change in comparison with the other commonly used algorithms.

Keywords: linear compressor; resonant frequency tracking; phase-locked loop; low-pass filter; PI regulator

*Corresponding author:
leimeizhen_lmz@163.com

Received 15 April 2021; revised 17 May 2021; accepted 23 May 2021

1 INTRODUCTION

Unlike the conventional rotary compressor that employs a crankshaft as the intermediate mechanism for converting the rotary motions from an induction motor to linear reciprocating motions to drive a compressor pump [1], the linear reciprocating compressor utilizes a linear reciprocating motor and resonant springs to directly drive the compressor piston and therefore has relatively high overall efficiency due to the elimination of the inherently frictional loss caused by the crankshaft mechanism in conventional rotary compressors [2]. The efficiency improvement of 10–20% has been demonstrated in linear compressors as compared with conventional rotary compressors [3]. The linear reciprocating compressor also offers significant advantages over its conventional counterpart including compact structure, higher controllability, lower vibration and noise and simpler modulation means. Therefore, the direct-drive linear compressor has attracted much attention recently and has been employed in household refrigeration appliances, thermoacoustic, vasculature and stirling regenerative cryogenic systems as a key component to save energy and reduce CO_2 emission [4].

The linear compressor operates most efficiently and requires the minimal electromagnetic force when its oscillation frequency equals the resonance frequency [5, 6]. Since the resonant frequency of the linear compressor is not only related to the mechanical spring elastic coefficient and the total mass of the actuator but also varies with the load, it is possible to make the linear compressor motor work under the resonant conditions by tracking the resonant frequency of the motor current. Therefore, the main goal of the linear compressor control is focused on how to track its resonant frequency of the linear compressor to achieve the efficient operations. The resonant frequency tracking approaches are thus very important in ensuring the highly efficient and reliable operations of the linear compressor under various working

International Journal of Low-Carbon Technologies 2021, 16, 1254–1263

https://doi.org/10.1093/ijlct/ctab047 Advance Access publication 16 June 2021

conditions. There have been several different kinds of resonant frequency tracking techniques developed for the linear compressors during recent years. A method of average value of stroke-current product (ASCP) for regulating the resonant frequencies of the linear compressor with a pulse-width modulation inverter was investigated in [7]. In [8], a system level controller was proposed to simultaneously achieve the stroke control and the resonance tracking by using nonlinear observers for gaining necessary information. The emphasis of the method was on the power factor and efficiency regulations based on the control of the average value of the product of the piston position and motor current. In [9], a model reference adaptive system-based resonant frequency tracking control algorithm was proposed, in which the system resonant frequency was directly calculated through the parameter adaptive rate. The effectiveness of the algorithm was verified by using simulation results. In [10], a learning feed-forward current controller consisting of a feedback proportional-integral controller and a feed-forward B-spline neural network was proposed for resonant frequency tracking of linear compressors. The steady state and transient performances of the controller were verified by using extensive simulation and experiment results. In [11], a resonant frequency tracking control strategy was proposed for a linear compressor to make the system resonant frequency vary with the force of gas compression. In [12], an adaptive resonant current controller was designed to allow the compressor to track the mechanical resonance frequency and simultaneously control the motor force. The controller was verified by simulation results. In [13], a phasor algorithm was proposed to calculate the natural frequency of the linear compressor. The calculated natural frequencies were verified by the tested motor efficiency. In [14, 15], a novel resonant frequency estimation method that calculates the phase difference between a supplied voltage and a mover position was proposed; the method calculates the phase difference by using the arctangent of a Fourier coefficient, which controls the drive frequency to keep the phase difference at 90°. The method was verified by experiment.

However, most of the conventional resonant frequency tracking methods depend on the steady state characteristics of the linear compressor. The existing resonant frequency tracking methods also mainly depend on the phase signal differences of the motor currents and piston position and demand the phase signal measurement of the motor currents and piston position individually. Since these phase signal measurements need at least half electrical period, the power supply frequency needs to be adjusted every half electrical period, which will slow down the response of the resonant frequency tracking. It is obvious that the current resonant frequency tracking methods suffer from the disadvantages of low response, complex operation and low anti-disturbance ability. The phase-locked loop (PLL) technology is usually used in phase synchronization and extraction, etc., and is widely used in power generation subsystem grid-connection [16, 17], motor control sliding mode observer angle calculation, etc. [18, 19].

In this paper, a novel PLL-based resonant frequency tracking control for linear reciprocating compressor is presented. By adopting a multiplier, low-pass filter and a PI regulator, the proposed PLL control method can be used to effectively and quickly track the resonant frequency and improve the system efficiency of the linear compressor under variable loading conditions. The operational principle, design and implementation procedure of the proposed method are detailed, and the performance of the proposed method is demonstrated by extensive simulation experiments in comparison with other commonly used algorithms.

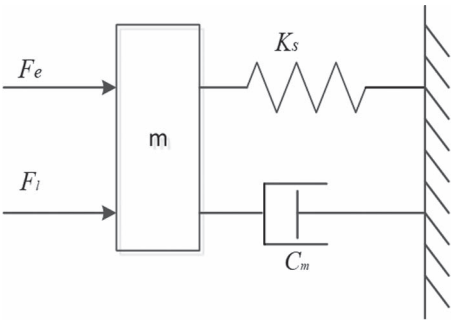

Figure 1. *Model of mechanical vibration system of the linear reciprocating compressor.*

The main contributions and innovations are as follows:

(1) The proposed resonant frequency tracking method does not require complex phase measurements and phase difference calculation, or the complex coordinate transformation, and can be easily implemented with high response speed.

(2) The proposed method can also achieve the tracking frequency control that is consistent with the current sampling frequency, which greatly improves the dynamic performance of the resonant frequency tracking response of the linear compressor under variable loading conditions.

(3) The proposed method can track the resonant frequency quickly and effectively, thus improving the system efficiency of the linear compressor under various loading conditions. Therefore, due to the significant advantages, the proposed method is deemed to be appropriate for the proposed compressor applications.

2 THE RESONANT FREQUENCY CONDITION

In order to derive the resonant frequency condition, the efficiency mathematical model of the linear reciprocating compressor system is conducted and analyzed. The linear compressor system reaches the maximum efficiency when operating frequency equals to the resonant frequency. Therefore, the resonant frequency tracking needs to be maintained in order to optimize the motor efficiency.

2.1. *Modeling of the linear reciprocating compressor system* [6]

The model of the linear reciprocating compressor system can be represented as Figure 1. According to Newton's second law, the dynamic equation of the mechanical system of the linear compressor can be obtained as shown in Equation (1), where

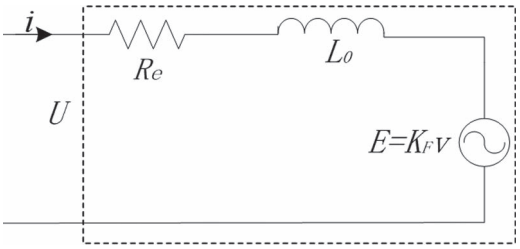

Figure 2. *Equivalent circuit diagram of linear oscillating actuator.*

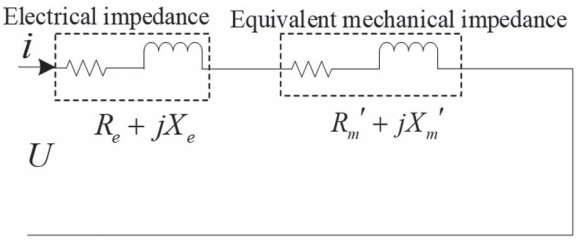

Figure 3. *Equivalent circuit diagram of linear oscillating actuator under load operation.*

m is the total mass of the actuator and F_l is the load force. During the movement of the compressor, the working medium of compression is refrigeration gas, which is a typical nonlinear gas force.

$$m\frac{d^2x}{dt^2} + c_m v + k_s x + F_l = F_e = k_F i \tag{1}$$

According to the equivalent circuit diagram in Figure 2, the voltage equation of the electromagnetic system is

$$u(t) = R_e i(t) + L_0\frac{di(t)}{dt} + k_F v \tag{2}$$

A linearized model of gas spring is usually employed to model the nonlinear gas force as shown in Equation (3), where k_g is the equivalent spring elasticity coefficient of the gas force and c_g is the equivalent damping coefficient of the gas force.

When the linear oscillating actuator drives the compressor load, and the gas pressure increases, the gas-force equivalent spring stiffness coefficient and gas-force equivalent damping coefficient will increase accordingly.

$$F_g = k_g x + c_g v \tag{3}$$

The linearized mathematical model of the electromechanical system when the linear oscillating actuator is loaded with a compressor can be obtained as

$$\begin{cases} m\frac{d^2x}{dt^2} + C\frac{dx}{dt} + Kx = k_F i \\ u = R_e i + L_0\frac{di}{dt} + k_F\frac{dx}{dt} \end{cases} \tag{4}$$

The pneumatic force is equivalent to the elastic force and damping force, which are superimposed into the actual elastic force and damping force as the following:

$$\begin{cases} C = c_m + c_g \\ K = k_s + k_g \end{cases} \tag{5}$$

Where K is the equivalent spring stiffness coefficient, C is the equivalent damping coefficient, under the non-load condition, $c_g = k_g = 0$.

2.2. *Analysis of the system efficiency* [9]

When the voltage source is designed as input, the voltage vector equation can be expressed as

$$\dot{U} = \dot{I}\left(R_e + jX_e\right) + \dot{E} = \dot{I}Z_e + k_F\dot{V} \tag{6}$$

According to the expression mode of velocity impedance, we obtain

$$\dot{V} = \frac{\dot{F}_e}{Z_m} = \frac{k_F\dot{I}}{Z_m} \tag{7}$$

Furthermore, the equivalent circuit of the linear oscillating actuator with mechanical load is shown in Figure 3.

Linear compressor is usually supported by a single-phase inverter, such that the motor current and voltage are single-phase AC quantities. The mathematical model of the system is written in phasor form as Equation (8), where ω is the system frequency.

$$\begin{cases} \dot{U} = R_e\dot{I} + j\omega L_0\dot{I} + k_F\dot{V} \\ -m\omega^2\dot{X} + j\omega C\dot{X} + K\dot{X} = k_F\dot{I} \end{cases} \tag{8}$$

The voltage–current relationship is

$$\dot{U} = \left[\left(R_e + j\omega L_0\right) + \frac{k_F^2}{C + (m\omega - K/\omega)}\right]\dot{I} \tag{9}$$

The input power is

$$P_i = \mathrm{Re}\left(\dot{U}\dot{I}^*\right) = \left[R_e + \frac{k_F^2 C}{C^2 + (m\omega - K/\omega)^2}\right]\left|\dot{I}\right|^2 \tag{10}$$

The output power is

$$P_o = \mathrm{Re}\left(\dot{F}_g\dot{V}^*\right) = \mathrm{Re}\left[\left(c_g\dot{V} + k_g\dot{X}\right)\dot{V}^*\right] = c_g\dot{V}\dot{V}^* \tag{11}$$

We have

$$P_o = \frac{k_F^2 c_g}{C^2 + (m\omega - K/\omega)^2}\left|\dot{I}\right|^2 \tag{12}$$

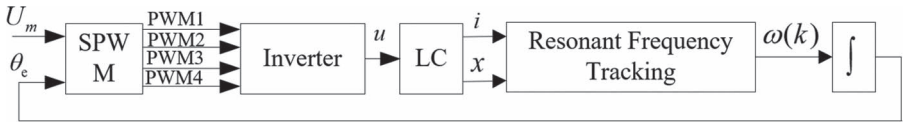

Figure 4. *The schematic of the linear compressor using the proposed resonant frequency tracking method, where LC denotes the line compressor.*

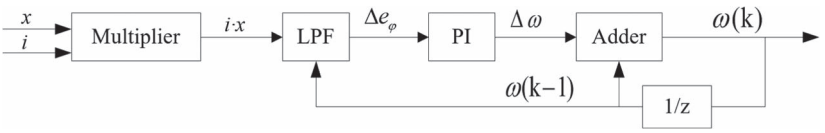

Figure 5. *The proposed resonant frequency tracking method, where LPF denotes the low-pass filter.*

Then, the efficiency is

$$\eta = \frac{P_o}{P_i} = \frac{k_F^2 c_g}{k_F^2 C + R_e\left[C^2 + (m\omega - K/\omega)^2\right]} \tag{13}$$

From Equation (11), it can be seen that the system reaches maximum efficiency condition when the operating frequency equals to $\sqrt{K/m}$, which is the resonant frequency. Moreover, the resonance frequency will vary with the equivalent spring elasticity coefficient k_g, which is contained in K. Therefore, the resonant frequency tracking control must be implemented to reach maximum efficiency condition. Furthermore, under resonance condition, the phase angle difference between piston position and motor current can be derived as

$$\dot{X} = \frac{k_F}{(K - m\omega^2) + j\omega C}\dot{I} \tag{14}$$

$$\theta_{x-i} = -\arctan\left(\frac{\omega C}{K - m\omega^2}\right) \tag{15}$$

It can be seen from Equation (15) that when system reaches resonant condition, the phase angle difference between piston position and motor current will equal 90°.

3 THE RESONANT FREQUENCY TRACKING CONTROL

The section presents the design of the proposed resonant frequency tracking method used in the linear compressor regulation. The operational principle, the design and the implementation procedure of the proposed method are detailed.

3.1. The proposed control method

Based on the principle of PLL, an error signal related to the phase difference between the piston position and motor current is constructed, and the power supply frequency is adjusted through the closed loop control to make the error signal equal to zero in order to realize the resonant frequency tracking control, while the phase difference is equal to 90°. As shown in Figure 4, the proposed novel resonant frequency tracking method is introduced in the linear compressor system to track the resonant frequency such that the line compressor (LC) works efficiently. The LC can be regulated by using an inverter driven by four channel PWM (pulse-width modulation) signals, which are generated by the SPWM (sinusoidal pulse-width modulation) algorithm.

The principle and structure of the resonant frequency tracking method are illustrated in Figure 5. As shown in the figure, the method mainly comprises a multiplier, a low-pass filter, a PI regulator and an adder. After the piston position signal and motor current signal pass through the multiplier and low-pass filter, the error signal of the PLL is generated as the input, and the power supply frequency is regulated by adjusting the power supply frequency to reach the resonant condition. Then, the input error signal of the PLL will converge to zero. The proposed method can be used directly on-line and in real-time to minimize the resonant frequency tracking error under all conditions.

The working principle of the proposed method is described as follows.

As shown in Figure 5, the instantaneous signal values of the motor current i and the piston position x are measured, respectively, then the product $(i \cdot x)$ of the signal values of the motor current i and piston position x are obtained through a multiplier. Consequently, the phase signal difference (Δe_φ) of the product can be obtained by passing the product signal through a low-pass filter.

The low-pass filtering is performed on the product signal $i \cdot x$ to obtain the error signal Δe_φ as Equation (16), where $\Delta\varphi$ is the phase difference signal.

$$\Delta e_\varphi = 2 \times LPF\,(i \cdot x) \propto \sin \Delta\varphi \tag{16}$$

As shown in Equation (16), the error signal Δe_φ is proportional to the sinusoidal value of the phase difference, which can be described as Equation (17), where φ_x is the phase of the piston position signal and φ_i is the phase of the current signal.

$$\Delta\varphi = \frac{\pi}{2} + \varphi_x - \varphi_i \tag{17}$$

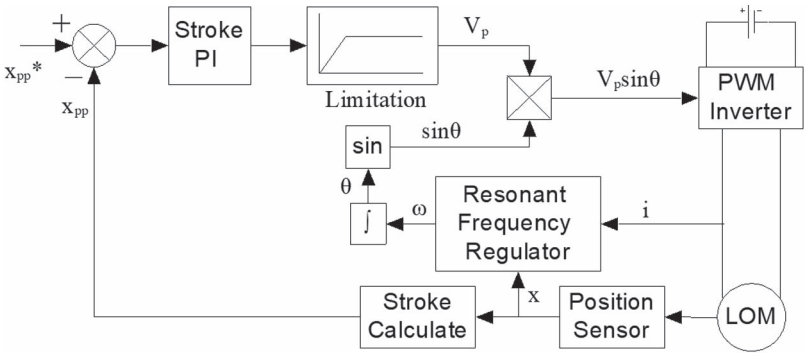

Figure 6. *The structure diagram of linear compressor control system.*

Then, as illustrated in Figure 4, based on the phase signal difference, the electrical frequency of the power supply can be adjusted through the PI regulator, that is, the SPWM (sinusoidal pulse-width modulation) frequency of the motor power supply can be adjusted until the steady-state tracking error signal is zero. Consequently, the power supply frequency of the linear compressor will be equal to its resonant frequency and the linear compressor works under the resonant conditions.

The working principle of the above method can be analyzed as follows:

The motor current and the piston position signals can be described as

$$i = i_m \sin(\omega t + \varphi_i) \tag{18}$$

$$x = x_m \sin(\omega t + \varphi_x) \tag{19}$$

where ω is the power supply frequency (rad/s), i_m is the amplitude of a sinusoidal current waveform and x_m is the amplitude of a sinusoidal piston position waveform.

Therefore, the product $(i \cdot x)$ can be described as

$$\begin{aligned} i \cdot x &= i_m \sin(\omega t + \varphi_i) \cdot x_m \sin(\omega t + \varphi_x) \\ &= -\frac{1}{2} i_m x_m [\cos(2\omega t + \varphi_i + \varphi_x) - \cos(\varphi_i - \varphi_x)] \end{aligned} \tag{20}$$

Moreover, the error signal Δe_φ can be calculated as

$$\begin{aligned} \Delta e_\varphi &= 2LPF(i \cdot x) = i_m x_m \cos(\varphi_i - \varphi_x) \\ &= i_m x_m \sin\left(\frac{\pi}{2} + \varphi_x - \varphi_i\right) = k \sin(\Delta\varphi) \end{aligned} \tag{21}$$

where k is the product of the amplitude of piston position signal waveform and that of the current signal waveform and *LPF* represents a digital low-pass filter, which can filter out the 2ω signal component of the frequency $i_m x_m \sin\left(2\omega t + \varphi_i + \varphi_x\right)$.

When the phase error $\Delta\varphi = \frac{\pi}{2} + \varphi_x - \varphi_i$ is relatively small, the relationship is as follows:

$$\Delta e_\varphi \approx i_m x_m \Delta\varphi \propto \Delta\varphi \tag{22}$$

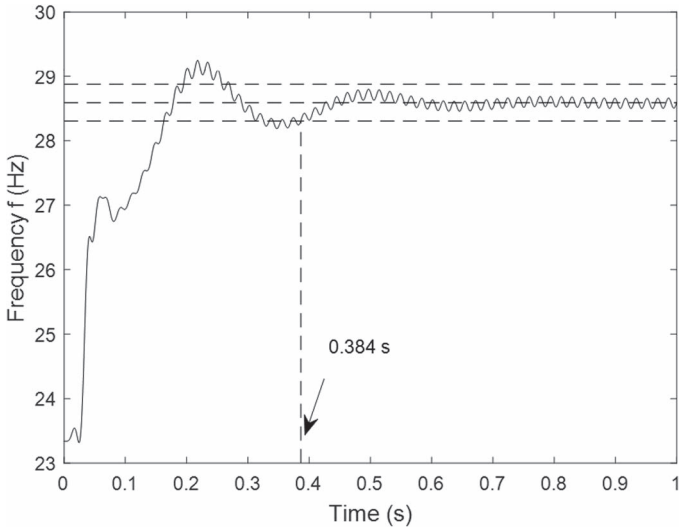

Figure 7. *Identification results of resonant frequency.*

When the phase error $\Delta\varphi = \frac{\pi}{2} + \varphi_x - \varphi_i$ is zero, that is, $\Delta e_\varphi = 0$, the phase difference between the motor current and piston position will be 90° (equal to $\pi/2$ in rad) and then the linear compressor reaches the resonant state. Hence, the resonant frequency tracking regulation of the linear compressor can be achieved by regulating the error signal to zero, i.e. $\Delta e_\varphi = 0$.

The above low-pass filter *LPF* is a first-order filter with variable cut-off frequency, and the cut-off frequency varies with the actual power supply frequency ω of the linear compressor, $\omega_c = \omega/M$ where $M = 1.0 \sim 10$. By using the low-pass filter with variable cut-off frequency, the high frequency (2ω) component in the product signal $i \cdot x$ that is independent of the error signal Δe_φ will be better filtered out.

The PI regulator adjusts the power supply frequency such that $\Delta e_\varphi = 0$. The regulator utilizes an incremental adjustment mode, that is, $\omega(k) = \omega(k-1) + PI(\Delta e_\varphi)$, where $\omega(k-1)$ is the power supply angular frequency of the previous control period and the initial value is the intermediate value within the operating frequency range of the linear compressor, that is, $\omega(0) = \omega_{\max}/2$.

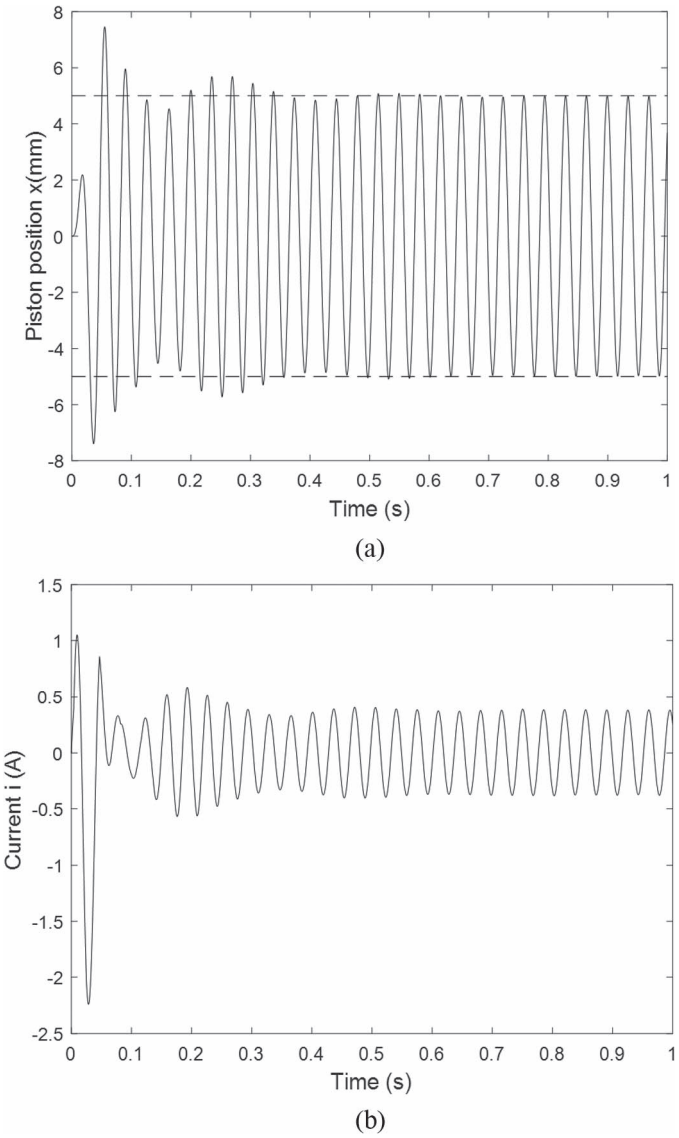

Figure 8. *Simulation results of piston position and motor current.*

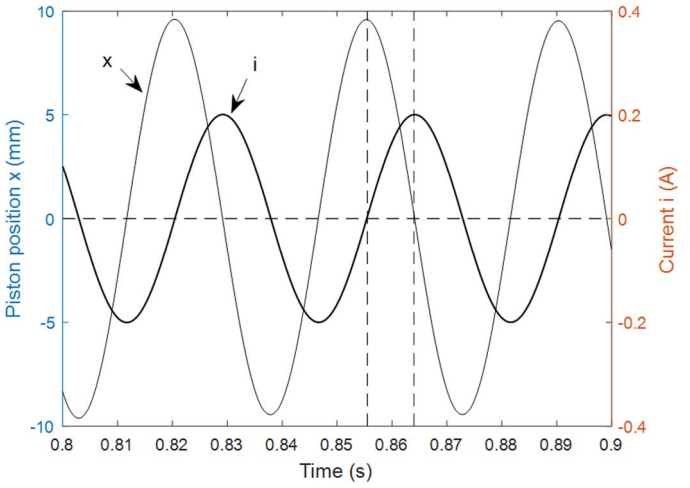

Figure 9. *Phase angle difference between piston position and motor current at steady state.*

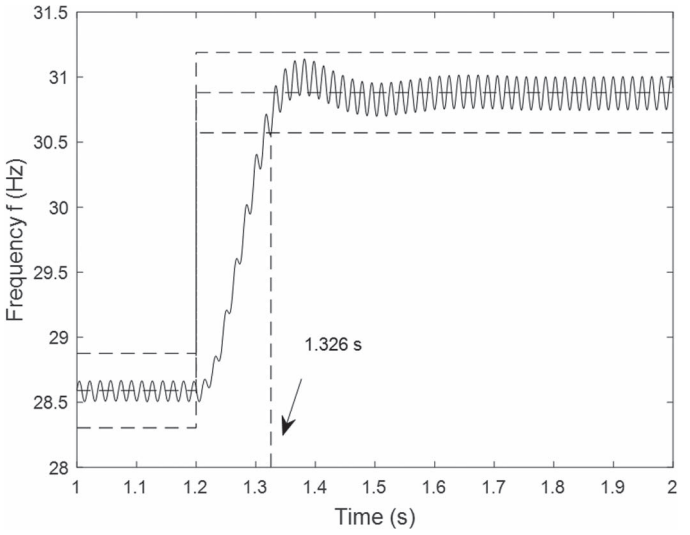

Figure 10. *Response of system resonant frequency.*

In addition, by keeping the voltage amplitude U_m of the linear compressor power supply unchanged, the voltage phase angle θ_e can be obtained by the integration of the power supply frequency ω with respect to time. Then, according to the power supply voltage amplitude U_m and voltage phase angle θ_e, the four channel PWM signals can be produced through the SPWM algorithm and can be used to control the inverter. Then, the single-phase AC inverter output can be generated to drive the linear compressor.

3.2. The implementation procedure

The proposed resonant frequency tracking method can be implemented in the LC system. In order to ensure that the LC operates under the resonant frequency condition over a wide range, a detailed implementation procedure is required. Therefore, the implementation procedure of the proposed method can be described as follows:

(a) Collect the instantaneous signal value of the stator current i of the linear compressor by using a current sampling chip. Collect the instantaneous signal value of the piston position x by using a resistance type position sensor.

(b) Obtain the product $(i \cdot x)$ through a multiplier.

(c) Consequently, the phase signal difference (Δe_φ) of the product can be obtained by passing the product signal through a low-pass filter.

$$\Delta e_\varphi = 2LPF\,(i \cdot x) \tag{23}$$

The transfer function of the digital low-pass filter can be described as

$$\Delta e_\varphi = 2LPF\,(i \cdot x) \tag{24}$$

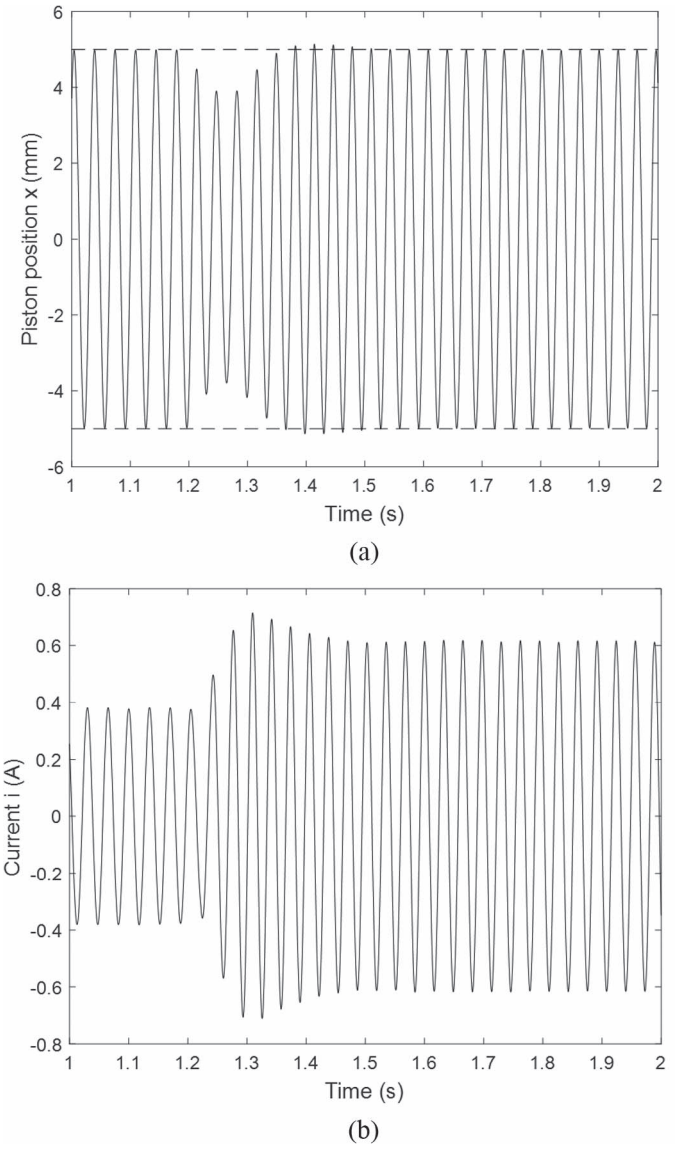

Figure 11. *Response of piston position and motor current.*

where the cut-off frequency $\omega_c = \omega/M$ and the value of M can be selected within the range of $1.0 \sim 10$.

(d) Then, use a PI regulator to adjust the power supply frequency such that the error signal Δe_φ converges to zero. The detailed procedure is as follows: when $\Delta\varphi > 0$, increase the power supply frequency; when $\Delta\varphi < 0$, reduce the power supply frequency; when $\Delta\varphi = 0$, keep the power frequency unchanged, that is, the current frequency is the resonant frequency.

By using the incremental PI regulator, namely, the output of PI regulator is added to the power supply frequency of the previous control state to obtain the current power supply frequency that needs to be applied, namely,

$$\omega(k) = \omega(k-1) + PI\left(\Delta e_\varphi\right) \tag{25}$$

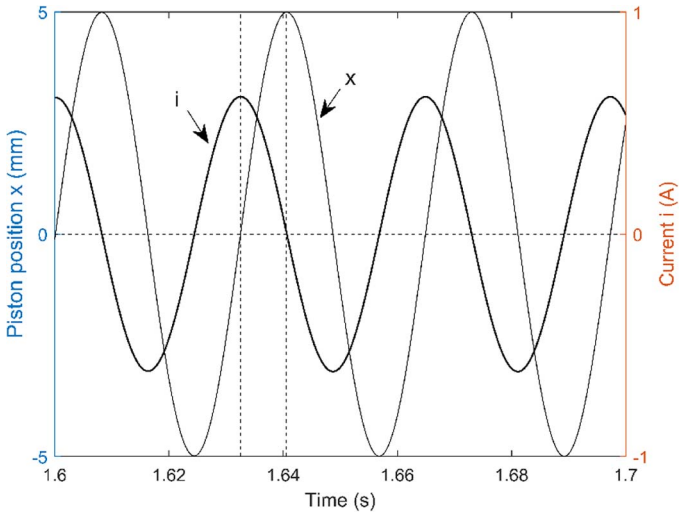

Figure 12. *Phase angle difference between piston position and motor current at new steady state.*

(e) Keep the voltage amplitude U_m of the compressor power supply unchanged; obtain the voltage phase angle θ_e through the integration of power supply angular frequency ω with respect to time. Then, according to the voltage phase angle θ_e and the voltage amplitude U_m, generate the four channel PWM signals through the SPWM algorithm for controlling the inverter such that the single-phase AC electrical output from the inverter can be produced to drive the linear compressor. The calculation formula can be designed as

$$\theta_e(k) = \theta_e(k-1) + \omega(k) \cdot T_s \tag{26}$$

where T_s is the control period, which is equal to the current sampling period.

4 RESULTS AND DISCUSSIONS

The performance of the proposed control method is verified through simulation experiments and comparisons with the commonly used algorithms. A linear compressor control system based on the ASCP [7] algorithm is also constructed in Simulink to demonstrate the advantages of the proposed algorithm.

4.1. Control system and startup performance

A linear oscillating actuator control system with the proposed method is constructed in Matlab/Simulink as shown in Figure 6.

The motor parameters in simulation are given as follows:

$R_e = 18\ \Omega$, $L_0 = 0.59$ H, $k_F = 47.08$ N/A, $m = 0.93$ kg, $c_g = 20$ N.s/m and $k_g = 30$ kN/m, i.e. the system resonant frequency is equal to 28.59 Hz. At startup, the target amplitude is set to 5 mm, and the system startup frequency is equal to 23.34 Hz, the PI controller parameters are as follows: $k_p = 20$, $k_i = 300$ for

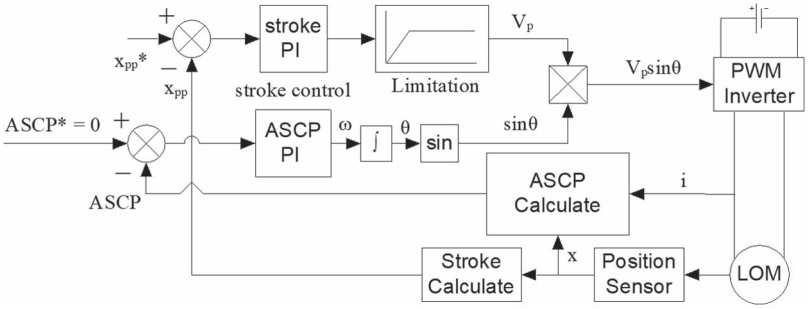

Figure 13. *Structure diagram of ASCP-based linear compressor control system.*

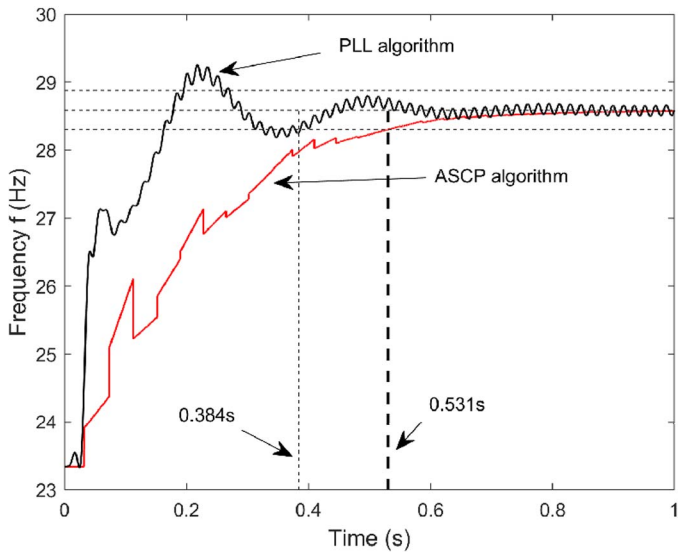

Figure 14. *Comparison of PLL algorithm and ASCP algorithm under the first type of operating condition.*

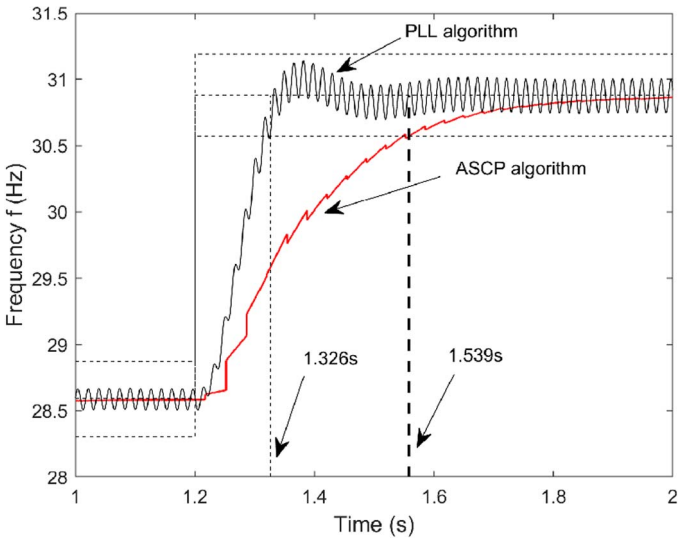

Figure 15. *Comparison of PLL algorithm and ASCP algorithm under the second type of operating condition.*

stroke controller; k_p = 1, k_i = 30 for frequency controller, M = 6 for the low-pass filter. In addition, the original piston position signal is amplified by 1000 times to improve the control accuracy.

As shown in Figure 7, the dotted lines represent the actual system resonant frequency of 28.59 Hz, and the ±1% settling time of the estimated system resonant frequency is 0.384 s, which demonstrates that the proposed method has the advantages of fast convergence speed and acceptable accuracy.

Figure 8 shows the response curve of piston position and motor current during startup process. Under PLL control strategy, the operating frequency quickly converges to the real system resonant frequency, and the spike current only appears at the startup instant. As shown in Figure 8, under the adjustment of the closed-loop stroke controller, the stroke value quickly reaches the target value with a small overshoot. Figure 9 illustrates that the steady-state phase angle difference between piston position and motor current is equal to 90°, which verifies the accuracy of the proposed PLL-based resonance frequency tracking control at startup.

4.2. Response to step load change

A sudden discharge pressure increase of the compressor causes a step load change. Several literatures indicate that the discharge pressure increase of linear compressors causes an increase of k_g and c_g. Therefore, the system equivalent spring coefficient K increases, which increases the system resonance frequency.

Figure 10 shows that the estimated resonance frequency value converges from initial value of 28.59 Hz to the target value of 30.88 Hz in 0.126 s, which verified that the proposed PLL-based resonance frequency tracking control has fast response speed and high convergence accuracy to step load change.

Figure 11 shows that under the adjustment of the stroke closed-loop controller, the stroke amplitude reaches the target value after about 0.3 s, and there is no spike in the current response. Figure 12 illustrates that the steady-state phase angle difference between piston position and current is still equal to 90°, which also verifies the accuracy of the proposed PLL-based resonance frequency tracking control at step load change.

4.3. Comparison with ASCP algorithms

Figure 13 shows the structure diagram of ASCP-based linear compressor control system; furthermore, the motor parameters, operating conditions and the control parameters of the stroke controller are the same as Section 4.1.

Figure 14 illustrates that at startup process, the PLL algorithm achieves ±1% error with a settle time of 0.384 s, while ASCP algorithm achieves ±1% error with a settle time of 0.531 s. The PLL algorithm has much faster convergence speed compared with the ASCP algorithm at startup process and decrease the setting time by about 27.7%.

Figure 15 shows that at step load change condition, the PLL algorithm achieves ±1% error with a settle time of 0.126 s, while ASCP algorithm achieves ±1% error with a settle time of 0.339 s. The PLL algorithm has much faster convergence speed compared with the ASCP algorithm at step load change condition and decrease the setting time by about 62.8%.

5 DISCUSSIONS

The slow convergence of the ASCP algorithm is due to using the ASCP value as a reference for frequency adjustment. A large ASCP value causes an increase of frequency adjustment rate, while a small ASCP value causes a reduction of frequency adjustment rate. However, the ASCP value is not only related to the phase angle difference between piston position and motor current but also related to the product of stroke and peak motor current.

At startup process, the ASCP value is very small due to that the stroke and motor current have not reached their steady state. Therefore, a lower frequency adjustment rate is adopted, which causes the ASCP algorithm to converge slowly. At step load change condition, the calculation of ASCP value requires the integration calculation in the oscillating period corresponding to the supply voltage frequency, while the sudden change in supply frequency causes the hysteresis and oscillation in the calculated ASCP value, which will lead to a decrease in the dynamic performance of resonant frequency tracking.

In the proposed PLL algorithm, by constructing the product signal of current and displacement, and performing low-pass filtering of the signal with variable cut-off frequency, a real-time error signal proportional to the phase angle difference of $i{\cdot}x$ is obtained. The refresh frequency of the real-time error signal is proportional to the current sampling frequency, which is much higher than the system oscillation frequency and can continuously reflect the phase angle difference between the piston position signal and motor current signal when the working conditions change. The voltage phase is adjusted by the PLL control to realize the resonant frequency tracking control. When the real-time error signal converges to zero, the resonant frequency tracking control is realized. Therefore, the proposed PLL algorithm has a much faster dynamic response compared with the ASCP algorithm.

6 CONCLUSION

In this paper, a novel PLL-based resonant frequency tracking method has been proposed for the linear compressor.

(1) The resonant frequency condition was derived by analyzing the efficiency model of linear reciprocating compressor system.

(2) The method proposed in this paper only needs the measurements of the instantaneous signal values of the motor current and the piston position.

(3) In the proposed method, a multiplier and a low-pass filter are used to obtain the phase signal difference, and then a PI regulator is used to make the phase signal difference converge to 90°. Therefore, the resonant frequency tracking and the high-efficiency resonant working conditions of the linear compressor can be achieved effectively.

(4) The detailed resonant frequency condition is analyzed and then the detailed design procedure of the proposed method is presented.

(5) The designed method and the resonant frequency characteristics of the proposed control method are verified by using the simulation experiment and comparisons with the other commonly used algorithms. The results indicate that the PLL algorithm achieves ±1% error with a regulation time of 0.126 s, while ASCP algorithm achieves ±1% error with a regulation time of 0.339 s.

The proposed method has been only verified by simulation, but there are no experimental results. In the future, the proposed method should be verified by experimental results, which will promote the industrial application of novel resonant frequency tracking control of the linear compressor.

CONFLICT OF INTEREST

To the best of our knowledge, the named authors have no conflict of interest, financial or otherwise.

ACKNOWLEDGMENTS

The work was supported by the Zhejiang Science Technology Department Public Service Technology Research Project under Grant No. LGF20E070001, Chinese National Natural Science Foundation under Grant No. 52003425 and the Fundamental Research Funds of Zhejiang Sci-Tech University under Grant No. 2019Q077.

REFERENCES

[1] Sultan IA, Phung TH. Improving torque performance in reciprocating compressors via asymmetric stroke characteristics. *Positive Displacement Machines, Academic Press*, 2019;145–62.

[2] Kun L. A review of linear compressors for refrigeration. *Int J Refrig* 2017;**84**:253–73.

[3] Hwang IS, Lee YL. Design of a high-efficiency linear compressor through a transient full-cycle CFD analysis. *Int J Appl Eng Res* 2014;**9**:26019–28.
[4] Zhang X, Ziviani D, Braun JE *et al.* Theoretical analysis of dynamic characteristics in linear compressors. *Int J Refrig* 2020;**109**:114–27.
[5] You XK, Qiu LM, Duan CX *et al.* Study on the stroke amplitude of the linear compressor. *Appl Therm Eng* 2018;**129**:1488–95.
[6] Lei MZ, Dai WZ, Wang LQ. Analysis on a novel halbach-type transverse-flux linear oscillatory motor for linear compressor. *Appl Mech Mater* 2013;**241-244**:1431–7.
[7] Chun TW, Ahn JR, Lee HH *et al.* A novel strategy of efficiency control for a linear compressor system driven by a PWM inverter. *IEEE Trans Ind Electron* 2008;**55**:296–301.
[8] Latham J, Mcintyre ML, Mohebbi M. Sensorless resonance-tracking and stroke control of a linear vapor compressor via nonlinear observers. *IEEE Trans Ind Electron* 2018;**65**:3720–9.
[9] Xu W, Wang Q, Li X *et al.* A novel resonant frequency tracking control for linear compressor based on MRAS method. *CES Trans Electr Mach Syst* 2020;**4**:227–36.
[10] Lin Z, Wang J, Howe D. A learning feed-forward current controller for linear reciprocating vapor compressors. *IEEE Trans Ind Electron* 2011;**58**:3383–90.
[11] Zhang T, Yu H. A novel strategy of resonant frequency tracking control for linear compressor. In *2017 20th International Conference on Electrical Machines and Systems (ICEMS)*. IEEE Press, 2017, pp. 1–6.
[12] Dainez PS, Oliveira JD, Nied A. An adaptive resonant controller applied to a linear resonant compressor. *Int J Refrig* 2019;**104**:521–29.
[13] Tang MS, Zou HM, Xu HB *et al.* Stroke and natural frequency estimation for linear compressor using phasor algorithm. *Int J Appl Electromagn Mech* 2014;**46**:763–74.
[14] Suzuki T, Koyama M, Nagata S *et al.* Resonant frequency tracking control for a linear compressor with assist springs. *2020 IEEE Energy Conversion Congress and Exposition (ECCE)*. IEEE Press, 2020, pp. 3016–21.
[15] Suzuki T, Koyama M, Nagata S *et al.* Position sensor-less resonant frequency estimation method for linear compressor with assist springs. In *2020 International Conference on Electrical Machines (ICEM)*, Vol. 1. IEEE Press, 2020, pp. 1206–12.
[16] Tomar KP, Kumar S, Singh B *et al.* Improved phase-locked loop-based control for grid-integrated PV system. *IET Renew Power Gener* 2020;**14**:705–12.
[17] Zou ZX, Liserre M. Modeling phase-locked loop-based synchronization in grid-interfaced converters. *IEEE Trans Energy Convers* 2020;**35**:394–404.
[18] Chen S, Zhang X, Wu X *et al.* Sensorless control for IPMSM based on adaptive super-twisting siding-mode observer and improved phase-locked loop. *Energies* 2019;**12**:1225–5.
[19] Duan JD. Instantaneous power control of a high speed permanent magnet synchronous generator based on a sliding mode observer and a phase locked loop. *Int J Electron* 2018;**105**:923–40.

浙江省科技计划项目

任 务 书

计 划 编 号： 2017C33160

项 目 名 称： 电梯门机智能定位控制系统关键技术研究

计 划 类 别： 公益技术应用研究

承 担 单 位： 浙江水利水电学院

项目负责人： 王立强

起 止 年 月： 2017-01-01 至 2018-12-31

浙 江 省 科 学 技 术 厅

2 0 1 6 年 制

填 写 说 明

1．本任务书文本适用于财政科技经费以“分期拨款”方式资助的一般科研计划项目、软科学研究项目。

2．本任务书所列内容应事实就是填写，表达要明确、严谨。

3．任务书中的“主要研发内容”，包括主要研发内容、关键技术及创新点等。

4．任务书中的“项目主要技术、经济指标”，包括项目完成时应达到的主要技术指标和水平、发表论文、申请获得专利等知识产权、人才培养及其他应考核的指标；技术及产品所形成的市场规模、生产能力、示范基地、产值、销售收入、利润等经济效益指标。公益类项目侧重于社会效益和潜在的经济效益指标。软科学研究项目需填写项目成果提供形式。

5．任务书中的“项目经费支出预算”，按《浙江省省级科技研发和成果转化项目经费管理暂行办法》（浙财教〔2012〕357号）规定的开支范围填写。

一、项目基本情况

<table>
<tr><td colspan="2">项目名称</td><td colspan="4">电梯门机智能定位控制系统关键技术研究</td></tr>
<tr><td colspan="2">项目主管处室</td><td colspan="2">社发处</td><td>项目主管</td><td>沈维强</td></tr>
<tr><td colspan="2">项目计划类别</td><td colspan="2">公益技术应用研究</td><td>技术管理领域</td><td>公共安全与防灾减灾</td></tr>
<tr><td colspan="2">归口管理部门</td><td colspan="2">浙江水利水电学院</td><td>项目技术来源</td><td>合作开发</td></tr>
<tr><td colspan="2">项目开始日期</td><td colspan="2">2017-01-01</td><td>项目完成日期</td><td>2018-12-31</td></tr>
<tr><td rowspan="5">承担单位</td><td>单位名称</td><td colspan="4">浙江水利水电学院</td></tr>
<tr><td>单位类型</td><td colspan="2">高等学校</td><td>法人代码</td><td>47004371-8</td></tr>
<tr><td>通讯地址</td><td colspan="2">杭州下沙高教园区学林街 583 号</td><td>邮政编码</td><td>310018</td></tr>
<tr><td>联系人</td><td colspan="2">朱一佳</td><td>手机</td><td>13777483600</td></tr>
<tr><td>电话/传真</td><td colspan="2">0571-86929153</td><td>E-mail</td><td>kejichu1211@163.com</td></tr>
<tr><td rowspan="2">合作单位</td><td colspan="3">单位名称</td><td colspan="2">法人代码</td></tr>
<tr><td>1</td><td colspan="3">宁波申菱电梯配件有限公司</td><td colspan="2">14501470-2</td></tr>
</table>

二、项目负责人及项目组成员

项目负责人	姓名	王立强	证件号码	612102198012133418
	学历	研究生	学位	博士
	职称	中级	现从事专业	电机与电器
	手机	15925638002	E-mail	flyingmind@163.com
	工作单位	浙江水利水电学院	法人代码	47004371-8
	通讯地址	杭州下沙学林街583号浙江水利水电学院	邮政编码	310018

	姓名	证件号码	所在单位	职称	从事专业	项目分工	年参加项目工作时间(月)
项目组成员	方贵盛	362334197307121217	浙江水利水电学院	正高	机械电子工程	参加	3
	邓成钢	370683197801280014	浙江水利水电学院	中级	机电一体化	参加	3
	王红梅	420922197806198624	浙江水利水电学院	副高	机械电子工程	参加	3
	张敏	340822198206301113	宁波申菱电梯配件有限公司	中级	电气工程及其自动化	参加	5
	葛文文	330225199004020347	宁波申菱电梯配件有限公司	中级	自动化	参加	5

三、主要研发内容

1、研发内容
该项目主要研发内容包括：电梯门机智能定位控制系统算法开发及仿真验证、算法驱动器硬件平台实现及调试、系统测试及运行测试。具体研发内容如下：
1） 算法开发及仿真验证
(1) SPMSM 全速度范围无编码器智能定位算法
a) 考虑饱和凸极及高频电感差异的 SPMSM 非线性建模；
b) 零速及中低速运行智能定位；
c) 中高速运行智能定位；
d) 中低-中高速过渡区域智能定位。
(2) SPMSM 全速度范围基于智能定位的矢量控制系统高精度定位控制算法
a) 上电初始位置智能定位；
b) 全速度范围矢量控制；
c) 引入速度及加速度前馈的矢量控制系统高精度定位控制。
(3) 基于智能定位的门机智能防夹算法
a) SPMSM 负载转矩自适应观测；
b) SPMSM 快速响应智能防夹。
(4) 基于智能定位的门机运行自适应防抖算法
a) SPMSM 负载转矩自适应观测；
b) 负载扰动补偿。
2） 算法驱动器硬件平台实现及调试
(1) 智能定位；
(2) 基于智能定位的矢量控制系统高精度定位控制。
3） 系统测试
(1) 空载；
(2) 地面对拖负载；
(3) 模拟门机系统（如图 3 所示）：在模拟门机的系统（接近实际门机工况）下，对门机智能定位控制系统功能、性能进行测试。
(4) 实际门机系统：在实际门机工况下，对门机智能定位控制系统功能、性能进行测试。
4） 运行测试
(1) 实际门机测试系统；
(2) 电梯井道实际门机系统。
2、项目关键技术
1） SPMSM 全速度范围无编码器智能定位技术；
2） SPMSM 全速度范围基于智能定位的矢量控制系统高精度定位控制技术；
3）基于智能定位的门机智能防夹技术；
4）基于智能定位的门机运行自适应防抖技术。
3、主要创新点
1）提出一种基于 SPMSM 全速度范围无编码器智能定位的门机矢量控制系统，实现电梯门机高精度智能定位控制；
2）提出一种基于防夹电流判断与自适应负载转矩观测判断相结合的门机夹人判断方

法，通过智能定位门机的高性能快速响应控制，实现门机智能可靠防夹；
3）通过自适应负载转矩观测，对负载转矩进行扰动补偿，实现基于门机智能定位的门机运行自适应防抖控制；
4）省去门机编码器，避免编码器故障导致电机、驱动器损坏从而引发的电梯门机安全事故，提高门机系统可靠性，进而提高电梯系统安全性。

四、项目成果提供形式

1、项目实施主要任务：
主要任务包括：电梯智能定位门机系统算法开发及仿真验证、算法驱动器硬件平台实现及调试、系统测试及运行测试。
2、目标
(1) 研发电梯智能定位门机驱动系统一套；
(2) 申请专利 3 项，其中发明专利 1-2 项；
(3) 发表研究论文 2-3 篇；
(4) 申报软件著作权 2 项。

五、项目经费来源

1、本项目研发总结费 15 万元，其中：甲方补助 15 万元，乙方自筹 0 万元，丙方配套 0 万元。
2、经费拨付和到位计划：

单位：万元

	首期	合计
甲方	15	15
乙方自筹	0	0
丙方配套	0	0

六、项目经费支出预算

单位：万元

经费开支科目		预算经费总额	其中省科技厅经费
一	直接费用	12.4	12.4
1	设备费	2	2
2	材料费	2.2	2.2
3	测试化验加工费	2	2
4	燃料动力费	0	0
5	差旅/会议/国际合作交流费	1.2	1.2
6	合作协作研究与交流费（国内合作）	0	0
7	出版/文献/信息传播/知识产权事务费	2	2
8	人员劳务费	2	2
9	专家咨询费	1	1
二	间接费用	2.6	2.6
10	间接费用(包含管理费与激励费)	2.6	2.6
合计		15	15

七、需增添的仪器设备

单位：万元

名称及规格型号	数量	单价	省科技厅拨款	自筹或其他	用途说明
NI 数据采集系统 NI USB-6343	1	2	2	0	数据采集分析对比

甲方(项目委托单位)：浙江省科学技术厅（盖章）

单位负责人（签字）：

2017 年 4 月 25 日

乙方（项目承担单位）：浙江水利水电学院（盖章）

项目负责人（签字）：王立强

单位负责人（签字）：

2017年 4 月 17 日

浙江省基础公益研究计划项目批准通知

王立强同志:

根据浙江省自然科学基金相关管理规定，浙江省自然科学基金委员会会同相关部门决定资助您申请的以下项目：

项目批准号	LGF20E070001		依托单位	浙江水利水电学院	
项目名称	直驱波浪能发电系统最优效率控制关键技术研究				
项目负责人	王立强		证件号码	612102198012133418	
项目类别	公益技术研究计划/社会发展		研究期限	2020 年 1 月 至 2022 年 12 月	
总经费（万元）	10.00	省财政资助经费（万元）	10.00	联合资助经费(万元)	0.00

序号	其他主要成员	证件号码	性别	单位名称
1	王红梅	420922197806198624	女	浙江水利水电学院
2	刘益军	330623197004240016	男	绍兴河悦机电设备有限公司
3	李明范	330106197601060415	男	浙江水利水电学院
4	邓成钢	370683197801280014	男	浙江水利水电学院
5	谢荣盛	421022198706012534	男	浙江水利水电学院
6	段震华	140302198711060031	男	浙江水利水电学院

浙江省自然科学基金委员会办公室

2019 年 11 月 19 日

浙江省基础公益研究计划项目批准通知
补办申请

项目负责人填写	申请理由： 项目负责人（签字）： 年　月　日
依托单位填写	依托单位科研管理部门审核意见： 负责人（签字）： （公章） 年　月　日

浙江省基础公益研究计划

项目计划书

立项编号	LGF20E070001		
项目名称：	直驱波浪能发电系统最优效率控制关键技术研究		
计划类别：	公益技术研究计划		
项目类别：	社会发展		
项目负责人：	王立强	电话：	15925638002
电子邮箱：	flyingmind@163.com		
通信地址：	浙江省/杭州市/江干区 . 下沙学林街 583 号		
邮政编码：	310018		
依托单位：	浙江水利水电学院		
联 系 人：	沈晓红	电话:	13858063930
申报日期：	2019-12-25		

浙江省科学技术厅

浙江省自然科学基金委员会

二 O 一九年制

填写说明

一、收到《浙江省基础公益研究计划项目立项通知》后，请认真阅读省基础公益研究计划有关项目和经费管理办法，按要求认真填写《浙江省基础公益研究计划项目计划书》（简称《计划书》）。填写《计划书》时要求科学严谨、实事求是、表述清晰、准确，并认真阅读本填报说明。

二、项目负责人应当按照申请书的内容填写《计划书》，除根据确定的资助额度对项目经费预算进行适当调整外，不得对申请书的其他内容进行变更。依托单位应对《计划书》内容进行审核。

三、《计划书》经项目负责人和依托单位签字盖章，并经省自然科学基金委员会办公室审核批准后，将作为项目执行、检查、验收的依据。

四、资助项目的有关研究成果，包括论文、专著、专利、获奖等情况，均须按规定标注“浙江省基础公益研究计划项目”（属于省自然科学基金的可标注“浙江省自然科学基金项目”）和立项编号。

五、省基础公益研究计划的项目经费管理（包括省级财政拨款经费、联合资助经费、自筹经费）依照省财政关于科技项目的有关经费管理要求执行，非省级财政拨款单位联合资助经费参照执行。

基本信息

负责人信息	姓　名	王立强	性别	男	出生日期	1980-12-13
	电 话	15925638002	E-mail		flyingmind@163.com	
	证件类型	身份证 18 位	证件号码		612102198012133418	

项目基本信息	项目名称	直驱波浪能发电系统最优效率控制关键技术研究		
	英文名称	Research on Key Technologies of Optimum Efficiency Control for Direct Drive Wave Energy Converter System		
	计划类别	公益技术研究计划	项目类别	社会发展
	项目研究阶段	应用研究		
	国家自然科学基金学科代码	E070303		
	国家自然科学基金学科代码名称	工程与材料科学部/电气科学与工程/电机与电器/电机及其系统		
	国家标准学科分类与代码	4704077		
	国家标准学科分类与代码名称	动力与电气工程/电气工程/可再生能源发电技术		
	预计研究年限	2020 年 1 月 至 2022 年 12 月		
	项目总经费	10.0 万元	其中省财政资助经费	10.00 万元
	中文关键词	直驱波浪能转换装置；最优效率模型；最优效率控制；锁相环控制；多目标优化		
	英文关键词	Direct-drive wave energy converter (DDWEC); Optimum efficiency model; Optimal efficiency control; Phase-locked loop control; multi-objective optimization		

中文摘要	项目研究内容与目标： 波浪能具有能流密度大、清洁、可再生等优点，浙江省波浪能资源潜在量在我国排名前四，波浪能开发利用前景广阔。直驱波浪能发电系统（Direct-drive Wave Energy Converter, DDWEC）省去中间传动环节，具有结构简单、系统效率高等优点，通过将多个 DDWEC 均匀分布在区域海平面上，可组成大功率波浪能发电场。在复杂海浪工况下，实现 DDWEC 实时、快速最大效率控制是波浪能发电领域急需解决的技术难题。为此，项目考虑直线发电机效率及系统输出限制，建立 DDWEC 最优效率输出模型，并提出基于锁相环的实时、快速最优效率捕获控制方法。项目综合应用水动力学、机械运动学、电磁学等理论，结合实验、多物理场有限元仿真分析及多目标优化方法，以考虑直线发电机效率及输出限制的 DDWEC 最优效率输出模型的建立及非规则波浪下 DDWEC 实时、快速最优效率控制方法等关键技术问题为突破口，建立反映 DDWEC 最优效率输出的功率输出装置（Power Take Off, PTO）最优阻尼及刚度系数与波浪频率的非线性关系模型，提出非规则波浪下基于最优效率输出模型及锁相环控制技术的 DDWEC 最优效率控制方法，并通过控制系统仿真及实验验证，解决直驱波浪能发电系统最优效率控制的关键技术问题，实现非规则海浪工况下 DDWEC 的实时、快速最优效率控制，将进一步推动我省波浪能开发利用进程。

项目组成员

编号	姓名	成员类别	出生日期	性别	单位名称	电话
1	王立强	负责人	1980-12-13	男	浙江水利水电学院	15925638002
2	王红梅	会员成员	1978-6-19	女	浙江水利水电学院	13958042396
3	刘益军	非会员成员	1970-4-24	男	绍兴河悦机电设备有限公司	0575-86282628
4	李明范	会员成员	1976-1-6	男	浙江水利水电学院	13067875683
5	邓成钢	会员成员	1978-1-28	男	浙江水利水电学院	13116741956
6	谢荣盛	会员成员	1987-6-1	男	浙江水利水电学院	18758063140
7	段震华	会员成员	1987-11-6	男	浙江水利水电学院	19817178632

项目经费

项目总经费 10.00 万元，其中省财政资助经费 10.00 万元（第一批财政拨款 10.00 万元，第二批财政拨款 0.00 万元），联合资助经费 0.00 万元，自筹经费 0 万元。

科研经费	名称	项目总经费预算（万元）
直接费用	1、设备费	0.00
	2、材料费	2.20
	3、测试化验加工费	2.50
	4、燃料动力费	0.00
	5、差旅费、会议费、合作、协作研究与交流费	1.80
	6、出版/文献/信息传播/知识产权事务费	1.00
	7、人员劳务费	1.00
	8、专家咨询费	1.00
间接费用	9、间接费用	0.50

需增添的仪器及设备：

名称	规格型号	数量	单价	金额(万)	资金来源	用途说明

研究计划

2020 年度
研究内容：（1）收集和整理资料，进一步完善和优化研究内容，并进行任务分解；
（2）做好实验前的准备工作，设计并完成实验平台的搭建；
（3）实验台架的改造、测试装置的建立以及直线波浪能转换装置的加工制造；
（4）理论分析，初步建立考虑直线发电机效率及输出限制的 DDWEC 最优效率输出模型。
（5）开展模拟不同波浪频率下 DDWEC 的流体、结构及电磁多物理场数值模拟分析，结合理论分析，完善考虑直线发电机效率及输出限制的 DDWEC 最优效率输出模型,导出 PTO 最优阻尼及刚度系数模型；
（6）进行内外特性实验，并根据测试结果辨识 PTO 最优阻尼及刚度系数模型。

研究目标：（1）完成论文 1 篇以上；
（2）参加国际学术会议及国内学术会议 1 次以上。

2021 年度
研究内容：开展非规则波浪下基于锁相环的 DDWEC 最优效率控制方法研究及控制系统仿真分析

研究目标：（1）完成论文 1 篇以上，参加国际学术会议及国内学术会议 1 次以上；
（2）完成实验平台搭建。

2022 年度
研究内容：开展非规则波浪下考虑发电机效率及输出限制的 DDWEC 最优效率控制实验研究
研究目标：（1）申报专利 2 项；
（2）申报软件著作权 2 项；
（3）成果鉴定及项目验收。

预期研究成果：

（1）开发直驱波浪能发电装置一套，系统具有如下技术指标：输出功率≥25W，系统效率≥25%.
（2）在国内外 SCI 或 EI 期刊上发表学术论文 2 篇；
（3）在直线波浪能转换领域申报发明专利 2 项，申报软件著作权 2 项。

研究年限期间预期完成的成果 6 项：

论著							
S(S)CI 收录	0	EI 收录	2	其他发表论文	0	专著	0
授权专利							
发明专利			2	实用新型专利	0	软件著作权数	2
参与制定完成的标准数							
国际	0	国家	0	行业	0	地方	0
推广应用情况							
新产品	0	新工艺	0	新技术	1	新品种	0
环境治理情况							
能耗			0	排放	0	水	0
土壤			0	空气	0	固废	0
人才培养情况							
研究期限内项目组成员晋升职称人数			1	研究期限内参与本项目的毕业研究生人数			0
社会公益情况							
对公共卫生起到明显作用			0	对食品安全起到明显作用			0
对社会治理起到明显作用			1	对防灾减灾起到明显作用			0

签字和盖章页

我接受浙江省基础公益研究计划的资助，将按照项目申请书、批准通知和计划书负责实施本项目，严格遵守浙江省基础公益研究计划相关项目和经费管理规定，切实保证研究工作时间，认真开展研究工作，按时报送有关材料，及时报告重大情况变动，对资助项目发表的论著和取得的研究成果按规定进行标注。

项目负责人（签字）：

年　月　日

我单位同意承担上述浙江省基础公益研究计划项目，将保证项目负责人及其研究队伍的稳定和研究项目实施所需的条件，严格遵守浙江省基础公益研究计划相关项目和经费管理规定，并督促实施。

依托单位（公章）：

年　月　日

浙江省自然科学基金委员会办公室审批意见：

同意。

浙江省自然科学基金委员会办公室

年　月　日

宁波大学 NINGBO UNIVERSITY

文献检索报告
SCI 收录

宁波大学图书馆（信息中心） **NBULIB**

报告编号：**202236000Z194059(S)**

数据库：科学引文索引 **(Science Citation Index Expanded)** 查证方式：文献被收录情况 时间范围：**1900** 年 **- 2023** 年	委托人：王立强 委托单位：浙江水利水电学院	检索人员：熊欢欢 检索日期：**2022**年**9**月**27**日

检索结果：被 **SCI** 收录文献 **2** 篇

#	作者	标题	来源出版物	出版物类型	入藏号
1	**Wang, LQ**; Wu, XQ; Lei, MZ	Feedforward-control-based nonlinear control for overhead cranes with matched and unmatched disturbances	***PROCEEDINGS OF THE INSTITUTION OF MECHANICAL ENGINEERS PART C-JOURNAL OF MECHANICAL ENGINEERING SCIENCE*** 2022, 236 (11): 5785-5795.	J Article	WOS:000748987200001
2	**Wang, LQ**; Wu, XQ; Lei, MZ	Continuous sliding mode control for the translational oscillator with a rotating actuator system	***TRANSACTIONS OF THE INSTITUTE OF MEASUREMENT AND CONTROL*** 2022, 44 (10): 1960-1967.	J Article	WOS:000747386500001
				合计	2

收录文献附录

第 **1** 条，共 **2** 条：

标题：Feedforward-control-based nonlinear control for overhead cranes with matched and unmatched disturbances

作者：Wang, LQ (Wang, Liqiang); Wu, XQ (Wu, Xianqing); Lei, MZ (Lei, Meizhen)

来源出版物：PROCEEDINGS OF THE INSTITUTION OF MECHANICAL ENGINEERS PART C-JOURNAL OF MECHANICAL ENGINEERING SCIENCE 卷：236 期：11 页：5785-5795 提前访问日期：JAN 2022 出版年：JUN 2022

文献号：09544062211063130

入藏号：WOS:000748987200001

文献类型：Article 出版物类型：J

作者地址：[Wang, Liqiang] Zhejiang Univ Water Resources & Elect Power, Fac Mech & Automot Engn, 928 Rd Two, Hangzhou 310018, Peoples R China.; [Wu, Xianqing; Lei, Meizhen] Zhejiang Sci Tech Univ, Fac Mech Engn & Automat, 928 Rd Two, Hangzhou 310018, Peoples R China.; [Lei, Meizhen] Zhejiang Univ, Suzhou Ind Technol Res Inst, Suzhou, Peoples R China.

通讯作者地址：Wu, XQ (通讯作者)，Zhejiang Sci Tech Univ, Fac Mech Engn & Automat, 928 Rd Two, Hangzhou 310018, Peoples R China.

第 **2** 条，共 **2** 条：

标题：Continuous sliding mode control for the translational oscillator with a rotating actuator system

作者：Wang, LQ (Wang, Liqiang); Wu, XQ (Wu, Xianqing); Lei, MZ (Lei, Meizhen)

来源出版物：TRANSACTIONS OF THE INSTITUTE OF MEASUREMENT AND CONTROL 卷：44 期：10 页：1960-1967 提前访问日期：JAN 2022 出版年：JUN 2022

文献号：01423312211069107

入藏号：WOS:000747386500001

文献类型：Article 出版物类型：J

作者地址：[Wang, Liqiang] Zhejiang Univ Water Resources & Elect Power, Fac Mech & Automot Engn, Hangzhou 310018, Peoples R China.; [Wu, Xianqing; Lei, Meizhen] Zhejiang Sci Tech Univ, Fac Mech Engn & Automat, Hangzhou 310018, Peoples R China.; [Lei, Meizhen] Zhejiang Univ, Suzhou Ind Technol Res Inst, Hangzhou, Peoples R China.

通讯作者地址：Wu, XQ (通讯作者)，Zhejiang Sci Tech Univ, Fac Mech Engn & Automat, Hangzhou 310018, Peoples R China.

检索人员：熊欢欢
教育部科技查新工作站（Z19）
2022年9月27日

浙江理工大学 ZHEJIANG SCI-TECH UNIVERSITY

浙江理工大学图书馆 **ZSTULIB**

文献检索报告
Retrieval Report

单号：**RT-2022-0905**

本次查收查引工作是根据委托人提供的作者姓名、组织机构及文献列表进行的，委托人信息如下：

姓名：王立强

机构：浙江水利水电学院

检索范围：

- 科学引文索引（Science Citation Index Expanded）： 1900年-2023年

检索结果：

检索类型	数据库	年份范围	记录数
SCI-E 收录	SCI-E	1900 - 2023	1

附件一：**SCI-E** 收录

#	作者	标题	来源出版物	出版物类型	入藏号
1	Wang, LQ; Yu, XF; Lei, MZ; Yin, XX	Novel phase-locked loop-based resonant frequency tracking control for linear reciprocating compressor	***INTERNATIONAL JOURNAL OF LOW-CARBON TECHNOLOGIES*** 2021, 16 (4): 1254-1263.	J Article	WOS:000744020200012
				合计	1

第 1 条，共 1 条：
标题： Novel phase-locked loop-based resonant frequency tracking control for linear reciprocating compressor
作者： Wang, LQ (Wang, Liqiang); Yu, XF (Yu, Xiaofan); Lei, MZ (Lei, Meizhen); Yin, XX (Yin, Xiuxing)
来源出版物： INTERNATIONAL JOURNAL OF LOW-CARBON TECHNOLOGIES **卷：** 16 **期：** 4 **页：** 1254-1263 **提前访问日期：** JUN 2021 **出版年：** DEC 2021
入藏号： WOS:000744020200012
文献类型： Article **出版物类型：** J
作者地址： [Wang, Liqiang] Zhejiang Univ Water Resources & Elect Power, Fac Mech & Automot Engn, 2nd St, Hangzhou 310018, Peoples R China.; [Yu, Xiaofan] Hangzhou NetEase Cloud Mus Technol Co Ltd, Res & Dev Ctr, Jianghong Rd, Hangzhou 310052, Peoples R China.; [Lei, Meizhen; Yin, Xiuxing] Zhejiang Sci Tech Univ, Fac Mech Engn & Automat, 2nd St, Hangzhou 310018, Peoples R China.
通讯作者地址： Lei, MZ (通讯作者)，Zhejiang Sci Tech Univ, Fac Mech Engn & Automat, 2nd St, Hangzhou 310018, Peoples R China.

详细结果请见附件。

检索人员：高 遐

浙江理工大学图书馆情报服务中心

2022年10月18日

浙 江 省 科 技 计 划 项 目
验 收 证 书

验收证书编号：浙科验字〔2019〕156号

计划编号：2017C33160

项目名称：电梯门机智能定位控制系统关键技术研究

计划类别：公益技术应用研究

完成单位：浙江水利水电学院

验收日期：2019年1月8日

浙江省科学技术厅

二OO六年制

二、承担单位

<table>
<tr><td rowspan="5">第一承担
单　位</td><td>单位名称</td><td colspan="10">浙江水利水电学院</td></tr>
<tr><td>所在地
代码</td><td>3</td><td>3</td><td>0</td><td>1</td><td>0</td><td>4</td><td>单位
类型</td><td>高等学校</td><td>代码</td><td>22</td></tr>
<tr><td>详细地址</td><td colspan="5">杭州下沙区学林街 583 号</td><td colspan="2">邮政编码</td><td colspan="3">310018</td></tr>
<tr><td>联系电话</td><td colspan="5">0571-86929153</td><td colspan="2">传　　真</td><td colspan="3">0571-86929153</td></tr>
<tr><td>归口部门</td><td colspan="10">浙江省水利厅、浙江省教育厅</td></tr>
<tr><td rowspan="9">合作单位</td><td colspan="2">单位名称</td><td colspan="8"></td><td>职责*</td></tr>
<tr><td>1</td><td colspan="8">宁波申菱电梯配件有限公司</td><td>测试技术支持</td></tr>
<tr><td>2</td><td colspan="8"></td><td></td></tr>
<tr><td>3</td><td colspan="8"></td><td></td></tr>
<tr><td>4</td><td colspan="8"></td><td></td></tr>
<tr><td>5</td><td colspan="8"></td><td></td></tr>
<tr><td>6</td><td colspan="8"></td><td></td></tr>
<tr><td>7</td><td colspan="8"></td><td></td></tr>
<tr><td>8</td><td colspan="8"></td><td></td></tr>
<tr><td rowspan="2">合作单位
总数 △</td><td colspan="3" rowspan="2">1</td><td colspan="4">承担单位数</td><td colspan="3">参加单位数</td></tr>
<tr><td colspan="4">0</td><td colspan="3">1</td></tr>
</table>

三、项目负责人及项目组成员

<table>
<tr><td rowspan="8">项　目
负责人</td><td>姓名</td><td colspan="7">王立强</td></tr>
<tr><td colspan="2">身份证号码</td><td colspan="6">612102198012133418</td></tr>
<tr><td>联系电话</td><td colspan="7">15925638002</td></tr>
<tr><td>E-mail</td><td colspan="7">flyingmind@163.com</td></tr>
<tr><td>学历</td><td>博士研究生</td><td>代码</td><td>11</td><td>学位</td><td>博士</td><td>代码</td><td>208</td></tr>
<tr><td colspan="2">专业技术职务</td><td colspan="2">工程师</td><td>代码</td><td>083</td><td>专业</td><td>电机与电器</td></tr>
<tr><td colspan="2">在本项目中的分工</td><td colspan="6">项目总负责，控制算法设计及实现</td></tr>
<tr><td>工作单位</td><td colspan="7">浙江水利水电学院</td></tr>
<tr><td rowspan="9">项目组
成　员</td><td>姓　名</td><td>出生年月</td><td>技术职务</td><td>专业</td><td>工作单位</td><td>在本项目中分工</td><td>年参加本项目工作时间</td></tr>
<tr><td>方贵盛</td><td>1973.7</td><td>正高</td><td>机械电子工程</td><td>浙江水利水电学院</td><td>算法的仿真验证</td><td>3</td></tr>
<tr><td>邓成钢</td><td>1978.1</td><td>中级</td><td>机电一体化</td><td>浙江水利水电学院</td><td>测试平台设计及加工</td><td>3</td></tr>
<tr><td>王红梅</td><td>1978.6</td><td>副高</td><td>机械电子工程</td><td>浙江水利水电学院</td><td>系统测试</td><td>3</td></tr>
<tr><td>张敏</td><td>1982.6</td><td>中级</td><td>电气工程及其自动化</td><td>宁波申菱电梯配件有限公司</td><td>测试系统设计技术指导</td><td>5</td></tr>
<tr><td>葛文文</td><td>1990.4</td><td>中级</td><td>自动化</td><td>宁波申菱电梯配件有限公司</td><td>门机系统功能技术指导</td><td>5</td></tr>
<tr><td></td><td></td><td></td><td></td><td></td><td></td><td></td></tr>
<tr><td></td><td></td><td></td><td></td><td></td><td></td><td></td></tr>
</table>

四、合同规定主要研究内容和目标

1 主要研究内容

主要内容包括：电梯智能定位门机系统算法开发及仿真验证、算法驱动器硬件平台实现及调试、系统测试及运行测试。

2 目标

（1）研发电梯智能定位门机驱动系统一套；

（2）申请专利 3 项，其中发明专利 1-2 项；

（3）发表研究论文 2-3 篇；

（4）申报软件著作权 2 项。

五、项目实施情况（包括技术目标实现情况、成果形式及应用等）

1 完成研究内容

（1）完成电梯门机智能算法设计及仿真验证

完成电梯门机用表贴式永磁同步电机（SPMSM）全速度范围无编码器智能定位算法及SPMSM全速度范围基于智能定位的矢量控制系统高精度定位控制算法的设计及仿真验证，仿真结果表明，电梯门机用SPMSM全速度范围无编码智能定位算法用于电机转子磁极位置及速度估计是可行的。

（2）完成算法驱动器硬件平台实现及调试

完成智能定位控制器的硬件平台搭建、控制算法的 DSP 代码设计、调试及验证及电梯门机系统测试平台的搭建工作。通过搭建与项目合作企业在用驱动器相当的基于TI F28035 DSP为核心的硬件驱动平台，平台经测试能可靠安全运行，为算法的实现提供可靠的硬件平台。通过 DSP 硬件平台驱动程序的开发及算法的代码实现，验证了SPMSM全速度范围智能定位控制算法，并实现基于该定位算法的高性能矢量控制系统软件开发、调试及硬件系统验证。电梯门机测试平台的搭建，为电梯门机智能定位控制系统提供与实际门机系统负载相同的工况。

（3）完成系统测试

在地面空载条件下，完成电机门机智能定位控制系统的控制功能（如模拟开门、模拟关门等操作）的测试，测试结果验证了算法的仿真结果，表明电梯门机智能定位控制算法可实现电梯门机电机的地面空载可靠运行，并实现模拟开门及关门操作。

（4）完成运行测试

完成电梯智能定位控制系统的在线运行测试，验证了开门功能、关门功能、重新开门功能、重新关门功能，测试结果表明电梯门机智能定位控制可用于电梯门机的可靠开门及关门测试运行。

2 解决了电梯门机智能定位控制系统如下关键技术

（1）SPMSM全速度范围无编码器智能定位技术；

（2）SPMSM全速度范围基于智能定位的矢量控制系统高精度定位控制技术。

3 项目目标完成情况

（1）完成一套电梯智能定位门机驱动系统研发，有检测报告；

（2）申报发明专利3项；

（3）发表论文4篇；

（4）申报软件著作权2项。

六、项目实现经济效益和知识产权情况

经济效益	年增产值（万元）	年增利润（万元）	年增税金（万元）	年创汇（万美元）	年节汇（万美元）
知识产权	科技论文（篇）	科技著作（种）	专利申请受理（件）	专利授权数（件）	其中发明专利数（件）
	4		3		

获奖情况	国家发明奖（项）	国家自然科学奖（项）	国家科技进步奖（项）	省部级科技进步奖（项）

七、项目资金使用情况

项目经费预算 15 万元，实际支出 14.346883 万元，结余 0.653117 万元，结余经费用于项目验收等后续支出。

（1）设备费 2.00 万元，用于购买项目立项合同中的 NI 数据采集卡，用于系统开发中的数据采集及分析处理。

（2）材料费，主要用于项目硬件平台及测试平台的材料费购买，尚有 0.001192 万元（11.92 元）结余。

（3）测试化验加工费用于项目硬件平台及测试平台的加工，尚有 0.0480 万元（480 元）结余。

（4）项目差旅费/会议/国际合作与交流费，主要用于项目相关的差旅及会议费，尚有 0.11385 万元结余。

（5）项目出版/文献/信息传播/知识产权事务费主要用于版面费、图书资料费、邮寄费及少量办公用品等费用的支出，尚有 0.000075 万元（0.75 元）结余。

（6）人员劳务费用于项目组成员外等临时雇佣的人员的劳务费的支出。

（7）专家咨询费主要用于项目研究及开发过程中的专家的咨询费的支出。

（8）项目间接费用除管理费外，其余用于项目组成员的激励费的发放，最后 1 个月由于年底单位额度用尽，提交的激励费申请单无法处理，尚有 0.49 万元结余。

八、验收意见

2019年1月8日，受浙江省科技厅委托，浙江水利水电学院组织专家对承担的浙江省公益技术应用研究计划项目“电梯门机智能定位控制系统关键技术研究”（计划编号：2017C33160）进行了会议验收。验收组审阅了相关材料，听取了项目组的工作总结、技术总结、经费决算和检测报告，经质询、讨论，形成验收意见如下：

一、提供的验收资料齐全、规范，符合验收要求。

二、项目完成了电梯门机智能定位算法的设计、仿真验证、实验验证及运行测试，解决了门机全速度范围无编码器智能定位及高精度定位控制问题，研发了一套电梯门机智能定位控制系统。项目研究成果简化了门机系统设计，降低了系统成本，提高了系统可靠性。

三、项目成果经浙江方圆检测集团股份有限公司检测（编号1811111240），验证了系统的可行性。

四、项目组发表论文4篇，申报专利3件，申报软件著作权2项，完成了项目合同书要求。

五、项目预算总经费15万元，全部为省财政科技补助经费，经浙江水利水电学院财务处决算，实际经费支出14.35万元，预计结余经费0.65万元，用于项目验收等后续支出。经费使用基本合理。

验收组认为，该项目已完成了项目合同书规定的内容和任务，同意通过验收。

验收组组长：

九、组织验收单位意见

浙江水利水电学院

十、验收组成员名单

姓　名	工作单位	现从事专业	职称/职称	签　名
王家军	杭州电子科技大学	电气工程	教授	
卢琴芬	浙江大学	电气工程	教授	
王文	杭州电子科技大学	机械工程	教授	
高金凤	浙江理工大学	控制工程	教授	
张薇兰	浙江省化工研究院有限公司	财务管理	高级会计师	